



Deposited via The University of Sheffield.

White Rose Research Online URL for this paper:

<https://eprints.whiterose.ac.uk/id/eprint/185857/>

Version: Accepted Version

Article:

Speers, L.J., Schmidt, R. and Bilkey, D.K. (2022) Aberrant phase precession of lateral septal cells in a maternal immune activation model of schizophrenia risk may disrupt the integration of location with reward. *Journal of Neuroscience*, 42 (20). pp. 4187-4201. ISSN: 0270-6474

<https://doi.org/10.1523/JNEUROSCI.0039-22.2022>

© 2022 the authors. This is an author-produced version of a paper subsequently published in *Journal of Neuroscience*. Uploaded in accordance with the publisher's self-archiving policy.

Reuse

Items deposited in White Rose Research Online are protected by copyright, with all rights reserved unless indicated otherwise. They may be downloaded and/or printed for private study, or other acts as permitted by national copyright laws. The publisher or other rights holders may allow further reproduction and re-use of the full text version. This is indicated by the licence information on the White Rose Research Online record for the item.

Takedown

If you consider content in White Rose Research Online to be in breach of UK law, please notify us by emailing eprints@whiterose.ac.uk including the URL of the record and the reason for the withdrawal request.

1
2
3
4
5
6
7
8
9
10
11
12
13
14
15
16
17
18
19
20
21
22
23
24
25
26
27
28

Aberrant phase precession of lateral septal cells in a maternal immune activation model of schizophrenia risk may disrupt the integration of location with reward

Authors

Lucinda J. Speers¹, Robert Schmidt³, David K. Bilkey^{1*}

¹Psychology Dept., Otago Univ. Dunedin, New Zealand, ³Psychology Dept., Univ. of Sheffield., Sheffield, United Kingdom.

Contact information: Professor David Bilkey, Department of Psychology, University of Otago, Dunedin 9054, New Zealand. Email: david.bilkey@otago.ac.nz

Number of pages: 41
Number of figures: 7
Number of words: Abstract – 249
Introduction – 655
Discussion – 1525

Declaration of interests

The authors declare no competing financial interests.

Acknowledgements

Support was provided through funding from the Health Research Council of New Zealand grant number 19/044.

29

Abstract

30 Spatial memory and reward processing are known to be disrupted in schizophrenia.
31 Since the lateral septum (LS) may play an important role in the integration of location and
32 reward, we examined the effect of maternal immune activation (MIA), a known
33 schizophrenia risk factor, on spatial representation in the rat LS. In support of a previous
34 study, we found that spatial location is represented as a phase code in the rostral LS of adult
35 male rats, so that LS cell spiking shifts systematically against the phase of the hippocampal,
36 theta-frequency, local field potential (LFP) as an animal moves along a track towards a
37 reward (phase precession). Whereas shallow precession slopes were observed in control
38 (CTL) group cells, they were steeper in the MIA animals, such that firing frequently
39 precessed across several theta cycles as the animal moved along the length of the apparatus,
40 with subsequent ambiguity in the phase representation of location. Furthermore, an analysis
41 of the phase trajectories of the CTL group cells revealed that the population tended to
42 converge towards a common firing phase as the animal approached the reward location. This
43 suggested that phase coding in these cells might signal both reward location and the distance
44 to reward. By comparison the degree of phase convergence in the MIA-group cells was weak,
45 and the region of peak convergence was distal to the reward location. These findings suggest
46 that a schizophrenia risk factor disrupts the phase-based encoding of location-reward
47 relationships in the LS, potentially smearing reward representations across space.
48

49

50

51

Significance statement

52 It is unclear how spatial or contextual information generated by hippocampal cells is
53 converted to a code that can be used to signal reward location in regions such as the ventral
54 tegmental area. Here we provide evidence that the firing phase of cells in the LS, a region
55 that links the two areas, may code reward location in the firing phase of cells. This phase
56 coding is disrupted in a maternal immune activation (MIA) model of schizophrenia risk such
57 that representations of reward may be smeared across space in MIA animals. This could
58 potentially underlie erroneous reward processing and misattribution of salience in
59 schizophrenia.

60

61 Previous studies suggest that the lateral septum (LS) integrates spatial and locomotor
62 information with reward (Bender et al., 2015; Luo et al., 2011; Wirtshafter & Wilson, 2019,
63 2020, 2021). The primary output of hippocampal CA1 cells that signal location (O'keefe &
64 Nadel, 1978) is to the LS (Risold & Swanson, 1997; Swanson & Cowan, 1977), and the LS in
65 turn has reciprocal connections to several regions involved in reward processing, including
66 the ventral tegmental area (VTA) and the striatum (Groenewegen, Vermeulen-Van der Zee,
67 Te Kortschot, & Witter, 1987; Luo et al., 2011; Zhang, Navarrete, Wu, & Zhou, 2022).
68 Consistent with this connectivity, the integrity of LS transmission is required for the
69 acquisition and flexible maintenance of conditioned place preferences (Cazala, Galey, &
70 Durkin, 1988; Jiang et al., 2018).

71 Recent work has shown that the LS uses both rate and phase coding to represent
72 location (Takamura et al., 2006; Tingley & Buzsáki, 2018; Wirtshafter & Wilson, 2020;
73 Zhou, Tamura, Kuriwaki, & Ono, 1999). For example, rate-coding cells that fire when an
74 animal is in a specific region of space, known as the cell's "place field" have been observed
75 in more dorsal regions of LS, although these place fields are not as robust as those observed
76 in the hippocampus (Takamura et al., 2006; Wirtshafter & Wilson, 2020). However, in more
77 rostral regions of the LS, cells display little evidence of rate coding but appear to encode
78 spatial location via phase precession (Tingley & Buzsáki, 2018).

79 Phase precession refers the observation that, as an animal moves through space, the
80 temporal spiking of principal cells systematically advances relative to the background theta
81 oscillation (O'Keefe & Recce, 1993; Skaggs, McNaughton, Wilson, & Barnes, 1996). When
82 phase precession occurs in an assembly of cells it produces theta sequences (Foster &
83 Wilson, 2007), thereby allowing for the sequential order of experience to be reproduced
84 within a compressed timescale that is suitable for synaptic plasticity (Dan & Poo, 2004). It
85 has been proposed that these phenomena underlie the sequential ordering of information that

86 evolves across time and space (Buzsáki & Tingley, 2018), and that they may play an
87 important role in learning and memory processes (Dragoi & Buzsáki, 2006; Jaramillo &
88 Kempter, 2017). These proposals have been supported by a growing body of work (Feng,
89 Silva, & Foster, 2015; Gupta, Van Der Meer, Touretzky, & Redish, 2012; Terada, Sakurai,
90 Nakahara, & Fujisawa, 2017; Wang et al., 2015; Wikenheiser & Redish, 2015), and recent
91 evidence has described phase precession and theta sequences in humans (Heusser, Poeppel,
92 Ezzayat, & Davachi, 2016; Qasim, Fried, & Jacobs, 2020).

93 Neurodevelopmental abnormalities and dysfunctional activity have been observed in
94 the septum of individuals with schizophrenia, including abnormal spiking activity and LFP
95 oscillations (Heath & Peacock, 2013; Heath & Walker, 1985). Furthermore, changes in LS
96 activity have been observed in both in vivo and in vitro studies following administration of
97 either antipsychotic or dissociative drugs in animal models (Contreras, Dorantes, Mexicano,
98 & Guzmán-Flores, 1986; Sheehan, Chambers, & Russell, 2004; Yu et al., 2002). The spatial
99 and contextual memory deficits (Brébion, David, Pilowsky, & Jones, 2004; Fajnerová et al.,
100 2014; Glahn et al., 2003; Hanlon et al., 2006; Park & Holzman, 1992; Rizzo et al., 1996;
101 Salgado-Pineda et al., 2016; Waters, Maybery, Badcock, & Michie, 2004; Weniger & Irle,
102 2008) and abnormal reward processing (Jensen et al., 2008; Strauss, Waltz, & Gold, 2013;
103 Whitton, Treadway, & Pizzagalli, 2015) that have been observed in schizophrenia may
104 therefore be linked to LS dysfunction.

105 In the present study we investigated whether a risk factor for schizophrenia,
106 maternal immune activation (MIA) altered LS activity. The MIA model is based on robust
107 epidemiological evidence that maternal infection during pregnancy increases the risk of
108 schizophrenia in the offspring (Adams, Kendell, Hare, & Munk-Jørgensen, 1993; Brown &
109 Meyer, 2018). When this is modelled in rodents, MIA animals have many schizophrenia-like

110 behavioral, cognitive and neural deficits (Bitanhirwe et al., 2010; Savanthrapadian et al.,
111 2013; Wolff, Cheyne, & Bilkey, 2011).

112

113 **Materials and methods**

114 ANIMALS AND EXPERIMENTAL DESIGN

115 All subjects were generated using the MIA intervention described previously by
116 Dickerson, Wolff, and Bilkey (2010), Wolff and Bilkey (2015) and Speers et al. (2021).
117 Female Sprague Dawley rats (~3 months old) were time-mated with GD1 considered to be
118 the first day after copulation. On GD 15, pregnant dams were anesthetized with isoflurane
119 (5%; Bayer) and administered either a single injection of polyinosinic:polycytidylic acid
120 (poly I:C; Sigma-Aldrich) 4.0 mg/kg, i.v. dissolved in 0.9% saline (Baxter), or an equivalent
121 saline injection 1 ml/kg. This dosage is the most common induction protocol used for rats
122 (Haddad, Patel, & Schmid, 2020). A number of previous studies have examined the precise
123 timing of injections on developmental phenotypes, with injections performed around GD 15
124 in rats leading to more robust phenotypes associated with schizophrenia than earlier injection
125 protocols, which have been associated more with autism spectrum disorders (Haddad et al.,
126 2020). Poly I:C and saline treatments were always performed in pairs.

127 Due to resource limitations, all litters were culled to a maximum of 6 male pups and
128 were housed in open cages prior to weaning. Post-weaning, male offspring were randomly
129 allocated a litter number and then housed in littermate groups of 2-3 in individually ventilated
130 cages (IVC). CTL and MIA animals were housed in a single housing room, which was
131 maintained at a normal 12-h light/dark cycle, and temperature controlled to 20-22°C. Juvenile
132 rats were provided with access to food *ad libitum*, and after 3 months were food deprived to
133 no less than 85% of their free-feeding weight in preparation for the experimental procedure.

134 Water was available *ad libitum* throughout the entire experimental procedure. All rats
135 weighed between 400 and 650g at the time of surgery.

136

137 APPARATUS AND TRAINING

138 Animals ran in a rectangular circuit measuring 900 by 800mm (Figure 1a). All arms
139 were 100mm wide with 270mm high side walls and constructed of wood. The entire
140 apparatus was painted in matte black and was devoid of visual cues. A video camera was
141 mounted on the ceiling of the recording room to view the whole apparatus. All experiments
142 were performed in a darkened environment with some ambient light from the recording
143 computer and a small lamp aimed away from the apparatus into one corner of the room.

144 The experimental procedure was identical to the procedure described previously in
145 Speers et al. (2021). Adult male offspring were randomly selected according to their litter
146 number, with a maximum of two animals per litter, and were trained over a period of 5 to 15
147 days. On days 1-5 rats were habituated to the recording room, apparatus and food reward, and
148 were allowed to free-forage for Coco Pops (Kellogg Company) scattered throughout the
149 apparatus. Following successful habituation, whereby rats actively explored the maze and
150 consumed the food reward, the placement of Coco Pops was gradually restricted, first to the
151 top 2 corners of the track and the centre of the reward arm, and then to the reward arm only.
152 During this period, rats were trained to run in a clockwise direction and were turned back to
153 the correct direction with a barrier when necessary. Coco-pops (approx. 6 per reward
154 delivery) were delivered manually by the experimenter. Training was considered completed
155 when rats consistently ran in a clockwise direction for the food reward over a twenty-minute
156 session.

157

158 SURGICAL PROCEDURES

159 All experimental protocols were approved by the Otago University Animal Ethics
160 Committee and conducted in accordance with New Zealand animal welfare legislation.
161 Following successful training, animals were anesthetized with 5% isoflurane (Merial New
162 Zealand) in oxygen and maintained at 1.5 to 2.5% throughout surgery. After animals were
163 anesthetized, they were given a subcutaneous injection of Atropine (1mg/kg) to ease their
164 breathing, as well as the analgesics Carprofen (1mg/kg) and Temgesic (buprenorphine;
165 0.1mL), and a prophylactic antibiotic, Amphoprim (trimethoprim and sulfamethazine,
166 0.2mL). Rats were then mounted on a stereotaxic apparatus (David Kopf Instruments) above
167 a heating pad, and a lubricating eye gel (Visine) was applied. The scalp was shaved and
168 sterilized with Betadine (Povidone-iodine), followed by a subcutaneous injection in the scalp
169 of the local anesthetic Lopaine (lignocaine hydrochloride 20mg mL⁻¹; 0.1mL diluted in
170 0.4mL of saline). After exposing the skull, two openings were drilled above the left
171 hemisphere, one above the dorsal CA1 region of the hippocampus, and one above the septal
172 region. A custom built, 8 channel, adjustable microdrive containing 1 tetrode and 1 tritrode
173 bundle of equal length was implanted at +.5mm AP, -1.5mm ML, and was lowered to ~4mm
174 from dura at an angle of ~7-8 degrees towards the midline (Figure 1b. Tetrodes consisted of
175 25µm nichrome, heavy formvar insulated wire (Stablohm 675 HFV NATRL; California Fine
176 Wire Company), and had been gold electroplated until impedances were reduced to ~200 –
177 300 kΩ (NanoZ, Neuralynx). A non-movable LFP electrode was separately implanted in CA1
178 at -3.8mm AP from bregma and -2.5mm ML from the midline, and then lowered to 2mm
179 from dura (Figure 1c). Microdrives were secured to the skull with jewellers' screws and
180 dental cement, and a ground wire was secured to an additional screw placed above the right
181 hemisphere. Post-surgery rats received a secondary dose of Amphoprim immediately upon
182 waking, and then an additional dose of Carprofen 24 hours later. Rats were provided with ad
183 libitum food and water post-surgery and were given 8 days to recover.

184

185 EXPERIMENTAL PROCEDURE AND ELECTROPHYSIOLOGICAL

186 RECORDINGS

187 Following recovery, rats were again food deprived to no less than 85% of their free-
188 feeding weight. Post-operative training and test trials were carried out in the recording room.
189 Rats were attached to a multichannel data acquisition system (DacqUSB; Axona Ltd), and
190 single unit data was closely monitored during test trials, which consisted of a 5-10 minute
191 recording session. Extracellular unit activity was first passed through an AC-coupled unity
192 gain amplifier before passing through to the recording system. Single unit data was bandpass
193 filtered between 600 and 6000 Hz, and sampled at a rate of 48 kHz with 24-bit resolution. For
194 each tetrode, one electrode with minimal spiking activity was selected as a reference. Action
195 potential thresholds were set at a minimum of 70 – 80 μ V and recorded for a 1 ms window
196 whenever the spiking amplitude was above this threshold. All spike events were time-
197 stamped relative to the beginning of the recording. LFP data was simultaneously recorded
198 from the CA1 region, was bandpass filtered up to 500 Hz (with notch filtering selective for
199 activity at 50 Hz) with a gain of \sim 500, and sampled at 48 kHz. The animal's location was
200 determined from 3 infrared LEDs mounted on the animal's head-stage and recorded by a
201 camera located above the chamber. Positional data was analysed with a sampling rate of 50
202 Hz and then converted into x and y coordinates by the recording system.

203 During the test period, tetrodes were slowly lowered (\sim 40 μ m per day) until well-
204 isolated single units were identified. Once single unit activity was confirmed, tetrodes were
205 lowered an additional \sim 40 μ m after every second recording for the remainder of the
206 experimental procedure. Experimental recordings were 20 minutes long, and testing
207 continued for \sim 3-8 weeks, until there was no further evidence of single unit activity, manual
208 adjustment had reached its limit, or the rat experienced other difficulties that terminated the

209 experiment. Final electrode placements are shown in Figures 1e and 1f. Rats ran no more
210 than one session per day, for ~60 – 80 laps per session. Single unit, position and LFP data
211 was saved for later analysis. All recordings with at least 1 putative place cell were included in
212 the final dataset.

213

214 ISOLATION OF SINGLE UNITS

215 For each recording, single units were identified manually offline using purpose
216 designed cluster cutting software (Plexon Offline Sorter, Version 3), primarily via the peak-
217 to-valley distance and principal components analysis of the waveforms. All stable waveforms
218 with clearly observed spike clustering were included in the initial analysis, regardless of
219 spike-width or firing rate. Example waveforms and cluster cutting from both CTL and MIA
220 recordings are presented in Figures 1d. Sorted data was then exported to MATLAB (version
221 R2019a, MathWorks), and analysis of single unit, position and LFP data was carried out in
222 MATLAB with custom-written scripts.

223

224 SELECTION OF FIRING ONSET LOCATION AND PHASE PRECESSION ANALYSIS

225 Initial inspection of firing properties around the track indicated that, although some
226 cells only fired in a portion of the track, the majority of cells fired indiscriminately across the
227 entire track. Where it did occur, the onset location of firing also appeared to vary from cell to
228 cell, and could appear at any point along the track. Due to this variability and lack of clear
229 place fields, manual selection of firing starting location and termination was used for phase
230 precession analysis. To these ends all cell recordings were split into groups of ~20 cells and
231 assigned a blinded identifier to ensure experimenter bias was minimized during the manual
232 selection process. These blind groups were then analysed with a custom MATLAB script that
233 first linearized the track, and then allowed the experimenter to select the start and end

234 locations of firing across 2 cycles of the track. For cells that only fired across a portion of the
235 track, firing onset and offset locations were always selected as the locations where robust
236 firing began and ended in a clockwise direction respectively. For cells that fired
237 indiscriminately across the entire track, the start location was selected on the basis of the
238 following criteria, in order: 1) a small pause in the firing, 2) the location where clear phase
239 precession could be observed to begin relative to random noise, and 3, if no clear firing
240 pauses or phase precession relative to noise were observed, then the analysis region was
241 always started just after the reward location, and ended just before the reward location.

242

243 DATA ANALYSIS

244 LFP activity recorded from electrode located in CA1 was sampled at 4800Hz. To
245 determine theta waveform shape, the LFP was bandpass filtered between 6-10Hz and a phase
246 profile was determined using the Hilbert transform. A sample waveform of 200 ms duration
247 was subsequently captured whenever the phase data indicated a trough had been reached.
248 These samples were then averaged, as were the related phase profiles.

249 Spatial information values, a measure of how informative a spike from a cell is
250 regarding the animal's current location within an environment, were calculated according to
251 the method described in Skaggs, McNaughton, and Gothard (1993). The formula for
252 information content, measured in bits per spike is:

$$Information = \sum_{i=1}^N p_i \frac{\lambda_i}{\lambda} \log_2 \frac{\lambda_i}{\lambda}$$

253 where the environment is divided into N distinct bins ($i = 1, \dots, N$), p_i denotes the
254 occupancy probability of bin i , λ_i is the mean firing rate for bin i , and λ is the overall mean
255 firing rate of the cell. Higher information values indicate that cells provide a more reliable
256 prediction of current location than cells with lower information values.

257 Correlations of hippocampal theta frequency and speed were generated for each
258 recording that showed evidence of single unit activity in the LS. This process involved
259 estimating instantaneous values for theta frequency from the Hilbert transform of LFP filtered
260 between 6 and 10 Hz. Estimates of instantaneous speed were determined by monitoring the
261 animals change in position over 500 ms time windows. Speed and theta frequency data were
262 then sampled at one second intervals and correlated. Samples where speed was below 5 cm/s
263 were excluded from the analysis.

264 For all phase precession analyses, the phase reference was always to the LFP signal
265 recorded from the non-movable electrode implanted in CA1, where a phase of zero
266 corresponded to the trough of the oscillation. Phase precession was determined by matching
267 the animal's position to the instantaneous phase of the 6-10 Hz theta rhythm at the CA1
268 reference, as determined from the Hilbert transform. These data were then analysed using
269 procedures described previously (Kempster et al., 2012; Speers et al., 2021). This involves
270 using circular-linear regression to provide a robust estimate of the slope and phase offset of
271 the regression line, and a correlation coefficient for circular-linear data analogous to the
272 Pearson product-moment correlation coefficient for linear-linear data. Phase precession
273 analysis was conducted by pooling spiking data from all passes through the region of interest
274 within a given recording session. The number of phase cycles per track was calculated as the
275 absolute value of the slope (in degrees per mm) multiplied by the length of the full track, and
276 then divided by 360. LS phase precession as described by Tingley and Buzsáki (2018) would
277 generally produce a value of around 1.

278 Correlations of firing rate and either speed or acceleration were based on the process
279 outlined by Wirtshafter and Wilson (2019). For this analysis, position was sampled every
280 100 ms to estimate instantaneous speed. These data were then smoothed across a 500 ms
281 window. The animals' occupancy per speed within 2cm/s bins was then established and then

282 spike count as a function of speed was determined. Spike count per speed was then divided
283 by speed occupancy to result in firing rate as a function of speed for each cell of interest.
284 Speeds with less than 2% of total occupancy were excluded from the analysis. The
285 correlation between speed and firing rate was assessed using a linear regression. Correlations
286 with acceleration were determined similarly except that a bin size of 0.5 cm/s^2 was used.

287 To allow between-animal comparison of phase trajectories across the track it was first
288 necessary that any phase shift that might have resulted from variation in the depth of the
289 hippocampal electrode was minimised. To this end the phase relationship between theta
290 activity recorded at the moveable LS electrode was compared to that recorded at the fixed
291 hippocampal electrode using cross correlation of LFP data filtered between 6-10Hz. It was
292 determined that phase shifted systematically as the LS electrode was lowered, but for some
293 animals this phase/depth relationship was offset at equivalent LS electrode depths. This
294 indicated that the depth of the reference hippocampal electrode was different between
295 animals, as theta phase varies depending on electrode position above and below the CA1 cell
296 layer (Brankač, Stewart, & Fox, 1993; Buzsáki, Rappelsberger, & Kellényi, 1985; Lubenov
297 & Siapas, 2009). With this information theta-frequency LFP phase difference between the
298 two electrodes was normalised to zero when LS electrodes were 4.5 mm deep from the dura
299 (see Figure 6b). All normalised phase trajectories were projected both forward and backwards
300 across the full extent of the linearized track. To determine whether there was any tendency
301 for phase trajectories to intersect at a particular location along the track, the phase angle of
302 each phase trajectory was determined in one cm increments along the track. A population
303 vector was then calculated for each location for all intercepting phase trajectories. The
304 subsequent population vector could vary from zero, indicating no clustering of phase
305 trajectories at this location, to one, which would indicate that all phase trajectories intersected
306 at one phase angle at that location.

307 To determine whether LS cells tended to fire in bursts at near-theta frequencies, an
308 autocorrelation of cell spiking with a +/-500 ms window was conducted across each
309 recording. The dominant frequency between 6 and 10 Hz was determined from the power
310 spectrum of the autocorrelation function.

311

312 HISTOLOGY

313 Following completion of experiments, animals were anaesthetised with 5% isoflurane
314 in oxygen, and a 2mA direct current was passed through each electrode for approximately 1
315 second to lesion the site of the electrode tip. Rats were then euthanized with an overdose of
316 isoflurane and transcardially perfused, first with 120 ml of 0.9% saline, and then 120 ml of
317 10% formalin in saline. Brains were then carefully extracted from the skull after removal of
318 the Microdrive, and stored in 10 % formalin in saline. One week prior to sectioning, brains
319 were transferred first to 10% formalin in H₂O for 24 hours, and then to a 10% formalin/30%
320 sucrose solution for approximately 3-7 days, until the brain sunk to the bottom of the sucrose
321 solution. Dehydrated brains were then sectioned into 60 µm coronal slices with a cryostat
322 (Leica CM1950). Sections were then mounted on slides and stained with a thionine acetate
323 Nissl stain (Santa Cruz Biotechnology, Inc. After slides were dry (min. 24 hours) electrode
324 placement was imaged with a local power (1.5x) digital microscope (Leica Biosystems, LLC)
325 to verify electrode placement (Figures 1e and 1f).

326

327 STATISTICAL ANALYSES

328 For all statistical analyses, we performed the following procedure. First, raw data was
329 transformed to a lognormal distribution if appropriate. All data (either in raw form or the log
330 transform) were then checked for assumptions of normality. These checks were performed in
331 GraphPad Prism 8.1.1 (GraphPad Software, Inc., San Diego, CA, USA), using the d'Agostino

332 & Pearson test for normality. If data did not meet the assumptions for normality based on the
333 d'Agostino & Pearson test, visual inspection of histograms and QQ plots was performed, and
334 extreme outliers were removed using the Graphpad function for removal of outliers. All data
335 that failed to meet assumptions of normality based on this procedure were then analysed
336 using the appropriate non-parametric test. Details about the specific tests used are provided in
337 the results section. All t-tests were two-tailed. Data with a normal distribution are presented
338 as mean \pm SEM unless explicitly stated otherwise in the figure legends. For all data that did
339 not meet normality assumptions, the median with 95% confidence intervals is depicted
340 instead. Significance levels were defined as $p < 0.05$. Additional information about
341 significance levels is provided in the figures as: * $p < 0.05$, ** $p < 0.01$, *** $p < 0.001$.
342 Additional circular statistics (to compare group differences in the intercept of the circular
343 correlation of phase and position, and to generate the MVL for animal by animal and litter by
344 litter analyses) were performed in Oriana 4 (Kovach Computing Services, Inc., Anglesey,
345 UK). Group differences for angular variance (defined as 1-MVL) were performed using the
346 variance ratio F-test, found at <https://www.statskingdom.com/220VarF2.html>

347

348 **Results**

349 *Tetrode verification in the rostral LS*

350 Single units were recorded from eight animals (7 litters) in both the CTL and MIA
351 groups respectively. However, one CTL animal was later excluded from further analyses due
352 to electrode misplacement in the medial septum (figure 1e). This decision was made not only
353 based on tetrode placement close to the MS, but also following inspection of other firing
354 properties suggesting that cells recorded from this animal were atypical. For example, cells
355 recorded from this animal had a significantly higher firing rate when compared to the average
356 firing rate of all other cells (figure 1e, lower right corner), and inspection of phase precession

357 plots showed that these cells were tightly coupled to specific phases of the LFP theta rhythm,
358 consistent with the firing properties of GABAergic medial septal neurons (Borhegyi et al.,
359 2004). After excluding this animal, a total of 144 units from seven CTL animals (6 litters)
360 and 362 units from eight MIA (7 litters) were used for all subsequent analyses. All animals
361 were age matched except for one pair, in which the CTL animal was seven months and the
362 corresponding MIA animal was twelve months, and one non-paired MIA animal (12 months).
363 All ages refer to animal age during experimental recordings, and ranged from 4 to 14 months.
364 There was no difference in the mean ages between groups (CTL = 10.43 ± 1.49 , MIA = 11.25
365 ± 1.13 , $t(13) = 0.45$, $p = 0.664$).

366

367 *Basic firing properties of LS cells, mean locomotor speed, and comparison of*
368 *hippocampal theta properties*

369 The median firing rate for all LS cells was 0.44 Hz, 95% CI [0.35, 0.51]. The
370 median log transformed firing rate was significantly higher for cells in the MIA group (-0.25,
371 95% CI [-0.34, -0.11]) than in the CTL group (-0.71, 95% CI [-0.80, -0.59], Mann Whitney U
372 =16638, $p < 0.001$; Figure 2a). Visual inspection of the distribution of firing rates around the
373 track indicated that activity was distributed relatively diffusely across the track for both
374 groups. In support of this observation, the spatial information content measure for all cells
375 was low (median = 0.69 bits/spike, 95% CI [0.59, 0.77]). It was, however, significantly lower
376 for cells in the MIA group (median = 0.59, 95% CI [0.51, 0.71]) compared to cells in the CTL
377 group (median = 0.82, 95% CI [0.71, 0.96], Mann Whitney U = 22555, $p = 0.007$; Figure 2b).
378 In a further quantification of spatial firing we identified the subset of cells where the
379 contiguous region of firing (as selected by the firing onset and offset locations) was less than
380 half the track length (<150cm), and where the spatial information content was greater than
381 0.8 bits/spike (Wirtshafter & Wilson, 2019). Only 4.7 and 5.8% of cells in the CTL and MIA

382 groups respectively met these criteria, confirming that spatially selective activity was rare for
383 both groups. There was no significant difference in these proportions between groups ($\chi^2(1) =$
384 0.54, $p = 0.46$).

385 The mean theta-frequency LFP amplitude recorded from electrodes located in the
386 CA1 region were significantly higher in the CTL group (M (log-transformed) = 3.17 ± 0.03 ,
387 MIA $M = 3.07 \pm 0.02$, $t(286) = 2.66$, $p = 0.008$; Figure 2d). The mean frequency of theta-
388 band CTL LFP recordings ($M = 7.92 \text{ Hz} \pm 0.02$) was also significantly higher than in MIA
389 recordings ($M = 7.72 \text{ Hz} \pm 0.02$, $t(286) = 7.0$, $p < 0.001$; Figure 2f), although the phase profile
390 was virtually identical for both groups (Figure 2h).

391 Mean running speed was significantly lower in the MIA group ($29.61 \text{ cm/s} \pm 0.50$)
392 than for the CTL group ($M = 31.42 \text{ cm/s} \pm 0.57$, $t(279) = 2.35$, $p = 0.02$; Figure 2c). To
393 determine whether this affected the theta-locomotion relationship (Bender et al., 2015) we
394 sampled hippocampal theta frequency and speed values once every second and computed the
395 correlation between these values for each individual recording. A comparison of the resultant
396 r values revealed that the median r value was slightly lower in the CTL group (median = 0.35,
397 95% CI [0.30,0.39]) when compared to the MIA group (median = 0.39, 95% CI [0.34, 0.24]),
398 but the difference was not significantly different (Mann Whitney $U = 8482$, $p = 0.059$),
399 although only marginally. There were no significant differences for either the slope of these
400 correlations (CTL $M = 6.97 \pm 0.38$, MIA $M = 7.36 \pm 0.31$, $t(284) = 0.80$, $p = 0.426$), or the
401 intercept (CTL $M = -37.12 \pm 3.02$, MIA $M = -39.86 \pm 2.49$, $t(284) = 0.7$, $p = 0.485$).

402

403 *LS cells in the MIA group continue to demonstrate robust phase precession, but are*
404 *more likely to precess through multiple theta cycles across the running track*

405 In total 34.03% of all cells in the CTL group and 30.12 % of all cells in the MIA
406 group showed evidence of significant phase precession (Figure 4a). This difference was not

407 statistically significant ($\chi^2(1) = 0.74$, $p = 0.391$). Examples are provided in Figure 3a (CTL)
408 and 3b (MIA). The circular-linear correlation of phase and position, as calculated across all
409 cells, was significantly higher in the CTL group (median = -0.07, 95% CI [-0.08, -0.05], MIA
410 median = -0.03, 95% CI [-0.04, -0.02], Mann-Whitney U = 21292, $p = 0.001$), although the p-
411 values of those correlations were not different between groups (CTL median = 0.162, 95% CI
412 [0.109, 0.269], MIA median = .244, 95% CI [0.191, 0.313], Mann Whitney U = 25017, $p =$
413 0.481). The same analyses were then performed on the subset of cells showing significant
414 phase precession. The difference between the circular-linear correlations for this subset was
415 non-significant although the result was marginal (CTL mean $r = -0.14 \pm 0.02$, MIA mean $r =$
416 -0.10 ± 0.01 , $t(156) = 1.94$, $p = 0.054$; Figure 4b). A similar, marginal result was obtained
417 for the p-value of the circular-linear correlation (CTL median = 0.004, 95% CI [0.001,
418 0.012], MIA median = 0.001, 95% CI [<0.001 , 0.003], Mann Whitney U = 2155, $p = 0.052$;
419 Figure 4c).

420 Visual comparison of phase precession trajectories across the track indicated that
421 many cells in the MIA group precessed through several theta cycles over the circuit (Figure
422 3b). By comparison this firing behaviour was observed in few cells from the CTL group.
423 Furthermore, when firing in MIA animals was analysed on a pass by pass basis, there were a
424 number of examples where firing cycled through more than 360 degrees, indicating that the
425 multiple-cycle precession was not simply a cumulative effect produced by variation on
426 individual passes (Schmidt et al., 2009). Analysis of the slope values obtained from the
427 circular-linear fit from all cells revealed that MIA group cells had a significantly steeper
428 slope when compared to CTL group cells (CTL median = -352 deg/mm, 95% CI [-435.7, -
429 188.3], MIA median = -522.2 deg/mm, 95% CI [-623.2, -468.1], Mann Whitney U = 20158,
430 $p < 0.001$; Figure 4d, left side). A similar result was obtained for the subset of cells
431 demonstrating significant phase precession (CTL median = -173.8 deg/mm, 95% CI [-351, -

432 122], MIA median = -526.4 deg/mm, 95% CI [-700, -424.9], Mann Whitney U = 1536, p
433 <0.001; Figure 4d, right side). The length of track over which these slope values were
434 calculated was not significantly different between groups (CTL median = 2662mm, 95% CI
435 [2523, 2871], MIA median = 2585mm, 95% CI [2468, 2815], Mann Whitney U = 2523, p =
436 0.581). By combining these slope values and the length of the track over which they were
437 calculated, it was possible to determine the number of phase precession cycles that would
438 occur across the entire track length, were precession to continue across the whole region. For
439 cells that demonstrated significant phase precession, the median number of phase precession
440 cycles in the CTL group was 0.79. This was significantly lower than the median number of
441 cycles in the MIA group (1.89 cycles, Mann Whitney U = 1562, p <0.001; Figure 4e).

442 To confirm that these slope differences were not a result of aberrant recordings from
443 a small proportion of MIA animals, mean values were also computed for each individual
444 animal and then compared across groups. For this analysis, only cells that demonstrated
445 significant phase precession were analysed. Comparison of slope values on an animal by
446 animal basis showed that MIA slope values were significantly steeper than CTL slope values
447 (CTL mean = -325.6 deg/mm \pm 50.28, MIA mean = -534.2 deg/mm \pm 69.81, $t(13) = 2.36$, p =
448 0.035; Figure 4f).

449 Dual oscillator theories of phase precession suggest that a change in the slope of
450 precession in MIA animals might result from an alteration in the theta-frequency/cell-burst-
451 firing-frequency relationship (Kamondi, Acsády, Wang, & Buzsáki, 1998; Magee, 2001;
452 Mehta, Lee, & Wilson, 2002; O'Keefe & Recce, 1993). To test this hypothesis, the burst
453 firing frequency of single cells was calculated. For both MIA and CTL groups mean burst
454 firing frequency was slightly higher than theta frequency, but there was no significant
455 difference in cell-burst frequency between the two groups (CTL median = 8.3 Hz, 95% CI
456 [8.06, 8.55], MIA median = 8.06 Hz, 95% CI [8.06, 8.06], Mann Whitney U 11452, p =

457 0.658; Figure 4h). As described previously, theta frequency was significantly lower in MIA
458 animals. As an approximation of how this difference might affect precession, for controls the
459 theta/burst relationship would result in cell firing precessing through a full 360 degrees in
460 approximately three seconds. In contrast, in MIA animals this precession would occur in
461 around 2.3 seconds. Thus, based on this difference MIA would precess around 30% faster
462 than control animals. This contrasts with the actual difference in precession cycles around the
463 track, which is closer to a 2-fold difference between MIA and controls (figure 4e).

464

465 *Starting phase is more variable for MIA cells when compared to CTL cells*

466 To determine the phase of cell firing as an animal enters the analysis region, the
467 intercept of the regression line for the circular linear-correlation was examined. Only cells
468 that demonstrated significant phase precession were included in this analysis. LS cells in both
469 the CTL and MIA groups demonstrated significant clustering at a mean phase angle of
470 314.83° (CTL Raleigh $Z = 15.78$, $p < 0.001$) and 288.96° (MIA Raleigh $Z = 12.36$, $p <$
471 0.001), around the starting phase. The circular variance of starting phase for MIA group cells
472 was, however, significantly greater than for CTL group cells (CTL = 0.43, MIA = 0.66, $F =$
473 0.43 , $p = 0.001$; Figure 4i). The Mardia-Watson Wheeler test, which considers group
474 differences in both the mean and variance for circular data, also returned a significant result
475 ($W = 8.99$, $p = 0.011$). As a further test, the circular distance from the mean angle was
476 computed for each cell and then compared across groups. Again, MIA group cells had a
477 significantly higher median distance from the mean angle when compared to CTL group cells
478 (Mann Whitney $U = 1996$, $p = 0.011$), indicating that precession starting phase was more
479 variable in the MIA group.

480

481 *Lead/lag times between the hippocampus and LS vary systematically according to*
482 *electrode depth*

483 Previous studies indicate that the firing phase of LS cells changes systematically
484 according to electrode depth (Tingley & Buzsáki, 2018). To examine this possibility, a
485 lead/lag analysis was performed for each recording to determine the phase shift of LS LFPs
486 when referenced to the non-movable hippocampal electrode. These results were then
487 correlated with LS electrode depth on an animal by animal basis (figure 5a). In the majority
488 of animals, the LS was more likely to lead the hippocampus at shallow depths, but as
489 electrode depth increased, the hippocampus was more likely to lead the LS. However, this
490 relationship was not always observed in the MIA group, with 3 animals showing the opposite
491 relationship. A t-test of the regression slopes of the depth/phase relationship indicated that
492 mean slopes were more positive in the CTL group ($M = 35.37 \pm 6.0$ when compared to the
493 MIA group ($M = 8.82 \pm 9.72$, $t(13) = 2.24$, $p = 0.043$). Inspection of the individual animal
494 phase and LS electrode depth relationship suggested that a number of animals (across both
495 groups) had greater hippocampal lead relative to depth (figure 5a). This was most likely due
496 to variability in hippocampal electrode depth (Brankačk et al., 1993; Buzsáki et al., 1985;
497 Lubenov & Siapas, 2009). To correct for this in further analyses, the phase of all recordings
498 was shifted, on a whole-animal basis, to align with a reference where zero phase shift
499 occurred at an electrode depth of 4500 microns (figure 5b).

500

501 *Relationship between firing phase and reward location*

502 In prior analyses LS cell phase precession had been examined across sections of the
503 track where firing occurred. As a result, data from different cells was often from different
504 (although often overlapping) regions of the track. To examine how the phase trajectories of
505 individual cells (the best fit to the firing phase-position data) would appear if precession was

506 assumed to continue from the start of the linearized track to the end, these phase trajectories
507 were normalized for differences in lead/lag likely resulting from variation in hippocampal
508 electrode position as described above, and then extended in each direction so as to cover the
509 whole track (Figures 5c and f). Inspection of these plots for CTL group cells indicated that a
510 large number of these individual phase trajectories tended to intersect near the location on the
511 track where the reward was delivered. To quantify this effect, each trajectory was allocated a
512 phase angle at each location on the track, based on the phase of firing at this location. Then
513 for each location on the track the average phase angle and mean vector length (MVL) across
514 the whole population of trajectories was determined. This procedure was repeated at one cm
515 increments along the whole track. The MVL thus provided a measure of the degree of
516 intersection of the phase trajectories at each location, which could vary from zero, indicating
517 no clustering of phase trajectories at that location, to one, which would indicate that all phase
518 trajectories intersected at that location. These resultant data indicated that CTL group MVL
519 was highest (0.50) at the reward location (Figure 5d). At the location with the highest MVL,
520 CTL group phase angles were significantly clustered with a mean phase angle of 200.06°
521 (Rayleigh $Z = 11.78$, $p < 0.001$; Figure 6e). When the same analysis was applied to the MIA
522 data, phase trajectories were overall less convergent (maximum $MVL=0.24$) with greatest
523 convergence occurring well prior to the reward location (Figure 5g). At the reward location
524 there was little evidence of convergence in MIA trajectories ($MVL = 0.08$; mean angle of
525 236.29° , Rayleigh $Z = 0.699$, $p = 0.497$; Figure 5h). A Mardia-Watson-Wheeler test revealed
526 significantly greater clustering at the reward location in the CTL compared to the MIA
527 groups ($MWW= 12.92$, $p = 0.002$).
528

529 *Firing rates of a substantial subset of cells located in the rostral LS are significantly*
530 *correlated with speed for both groups, but positive correlations were significantly more*
531 *frequent in the MIA group*

532 Recent work has demonstrated that the dorsal LS contains a population of cells for
533 which firing rate has a strong linear relationship with either speed or acceleration (Howe &
534 Blair, 2020; Wirtshafter & Wilson, 2019). To examine whether cells located in the rostral LS
535 are also modulated by speed, we computed Pearson correlations of speed and firing rate for
536 each cell (example correlations are provided in Figure 6a. In total, just over 30% of all CTL
537 group cells had firing rates that were significantly correlated with speed, in contrast to almost
538 45% of all MIA group cells. These proportions were significantly different ($\chi^2(1) = 8.6$, $p =$
539 0.003). From these significant subsets, 45% of all cells in the CTL group and 59% of cells in
540 the MIA group had firing that was positively correlated with speed (Figure 6b). Again, these
541 proportions were significantly different between groups ($\chi^2(2) = 10.61$, $p = 0.005$). When the
542 absolute median r-values generated by these correlations were compared across the entire
543 dataset, they were also significantly higher in the MIA group (CTL median = 0.41, 95% CI
544 [0.31, 0.51], MIA median = 0.56, 95% CI [0.51, 0.60], Mann Whitney U = 20426, $p < 0.001$:
545 Figure 6c). The median r-values were also compared separately according to the direction of
546 these correlations for those data where significant correlations between firing rate and speed
547 were observed. Results from this reduced data subset showed that there were no group
548 differences for the median r-values for either positive correlations (CTL median = 0.77, 95%
549 CI [0.69, 0.88], MIA median = 0.81, 95% CI [0.78, 0.85], Mann Whitney U = 861, $p = 0.517$)
550 or negative correlations (CTL median = -0.75, 95% CI [-0.80, -0.70], MIA median = -0.79,
551 95% CI [-0.81, -0.74], Mann Whitney U = 674, $p = 0.245$, Figure 6c).

552 To test the possibility that spatial and locomotor information map onto distinct cell
553 populations, the group of cells demonstrating significant phase precession (“phase coding

554 cells”) was compared with the group of cells that had firing rates significantly correlated with
555 speed (“speed modulated cells”) to determine if there was any overlap. Of the 49 phase
556 coding cells in the CTL group, 18 were also speed modulated cells, including 12 cells with a
557 positive speed correlation. In total, only 24% of all CTL group cells that had either phase
558 coding or speed modulated properties were involved in both these processes simultaneously.
559 In the MIA group, 59 out of 109 phase coding cells were also classed as speed modulated
560 cells, including 43 cells with positive speed correlations (Figure 6d). In total, this amounted
561 to 28% of cells with overlapping coding properties. These proportions were not significantly
562 different between groups ($\chi^2(1) = 0.41$, $p = 0.52$).

563 The firing of a relatively small proportion of cells were modulated by the animal’s
564 acceleration. In total 8% of CTL group cells and 9% of MIA group cells displaying a
565 significant correlation with either acceleration or deceleration (Figure 6e). These proportions
566 were not significantly different between groups ($\chi^2(2) = 1.57$, $p = 0.456$). The difference
567 between the absolute r-values were also not significant for either acceleration (CTL median =
568 0.25, 95% CI [0.17, 0.29], MIA median = 0.24, 95% CI [0.19, 0.28], Mann Whitney U =
569 14400, $p = 0.657$) or deceleration (CTL median = 0.23, 95% CI [0.21, 0.27], MIA median =
570 0.22, 95% CI [0.20, 0.26], Mann Whitney U = 24385, $p = 0.673$; Figure 6e), and similar
571 results were obtained when only those cells with significant correlations were included in the
572 analysis (for acceleration, CTL $M = 0.67 \pm 0.03$, MIA $M = 0.74 \pm 0.05$, $t(18) = 1.07$, $p =$
573 0.299 ; for deceleration, CTL $M = 0.64 \pm 0.05$, MIA $M = 0.66 \pm 0.04$, $t(20) = 0.21$, $p = 0.834$).

574

575 **Discussion**

576 We investigated whether MIA altered neuronal coding of location in the rostral LS, a
577 region which is likely to provide an important link between location coding mechanisms and
578 reward systems (Bender et al., 2015; Luo et al., 2011; Wirtshafter & Wilson, 2019, 2020,

579 2021). Most cells fired indiscriminately across the majority of the track, with only a small
580 proportion of cells (~5%) in both the CTL and MIA groups showing evidence of spatially
581 selective firing reminiscent of place cells. This is consistent with previous reports that
582 sampled cells from the rostral LS (Tingley & Buzsáki, 2018) and contrasts with prior studies
583 targeting the dorsal LS, where LS “place fields” (Wirtshafter & Wilson, 2020) (Takamura et
584 al., 2006) have been described. These data therefore provide corroborating evidence that the
585 rate coding of location varies across LS sub-regions.

586 Approximately a third of all LS cells displayed evidence of significant phase coding
587 of location across both groups. This is considerably less than the 89% of cells reported to
588 display phase coding in the Tingley and Buzsáki (2018) study. It should be noted, however,
589 that they used different criteria to determine whether cells showed evidence of phase coding,
590 and our methodology is likely more conservative. During phase coding in CTL cells the
591 phase of firing typically precessed across a single theta cycle as animals navigated the full
592 length of the track (Tingley & Buzsáki, 2018). In contrast, although the MIA manipulation
593 did not compromise the ability of LS cells to precess, there was a significantly steeper slope
594 of precession. In many cells, this resulted in phase precession that circulated through several
595 360-degree cycles as the animal traversed the track. Phase precession in excess of a single
596 theta cycle has not generally been observed in previous studies of the phenomenon (Dragoi &
597 Buzsáki, 2006; Ekstrom, Meltzer, McNaughton, & Barnes, 2001; Geisler et al., 2007; Huxter,
598 Burgess, & O'Keefe, 2003; Kamondi et al., 1998; Kjelstrup et al., 2008; Maurer et al., 2006;
599 O'Keefe & Recce, 1993; Royer, Sirota, Patel, & Buzsáki, 2010; Schmidt et al., 2009; Skaggs
600 et al., 1996; Terrazas et al., 2005; Tingley & Buzsáki, 2018). Instead, phase range has been
601 shown to dynamically shift according to either place field size or route familiarity across a
602 range of experimental paradigms so that that precession remains restricted to 360 degrees
603 across a place field (Ekstrom et al., 2001; Kjelstrup et al., 2008; Royer et al., 2010; Terrazas

604 et al., 2005). It is possible that the multiple phase precession cycles observed in the MIA
605 group represent more discrete “place fields” that are entirely decoupled from firing rate, with
606 discrete “fields” anchored to salient features of the animal’s current environment or specific
607 task demands (Gupta et al., 2012; Maurer et al., 2006). In contrast, CTL animals may be more
608 likely to collate these discrete environmental “chunks” into a coherent whole as the animal
609 becomes more familiar with a learned navigational route (see figure 7).

610 When CTL phase trajectories were projected across the full length of the track, as a
611 population they tended to converge so that LS cells were firing at around the peak of theta
612 activity as recorded at the CA1 cell layer. This convergence was maximal at the location of
613 reward delivery. In contrast there was no evidence of phase trajectory convergence at the
614 reward region in MIA animals. The one previous paper that has described and examined
615 phase coding in the LS concluded that the LS phase code was likely agnostic to reward
616 location, however, this analysis was not a major focus of the paper, and some neurons were
617 clearly linked to local cues such as the goal (Tingley & Buzsáki, 2018). Our finding
618 contributes to a growing body of evidence indicating that the LS is involved in the integration
619 of spatial and reward information (Bender et al., 2015; Luo et al., 2011; Wirtshafter &
620 Wilson, 2019, 2020, 2021), and similar to phase precession in the ventral striatum, suggests
621 that firing phase in the LS may contain information about reward proximity or salience (van
622 der Meer & Redish, 2011). It should be noted, however, that we did not systematically
623 manipulate reward location in our study, to isolate it from other local cues. Further study
624 would be required to test this hypothesis.

625 If phase of firing signals reward location and distance to reward then we would
626 predict that in the MIA animals the association between reward and location is ‘smeared’
627 across the environment such that a far broader range of stimuli and locations become
628 associated with the reward. Since the LS has direct connections to the VTA, this effect may

629 model, and potentially provide a mechanism for, some of the changes observed in
630 schizophrenia (Zhang et al., 2022). In particular altered motivational salience (Kapur, 2003),
631 which occurs with dysregulated dopamine signals and a tendency for individuals to mis-
632 assign salience to the elements of experience.

633 One of the most salient landmarks available to animals in this study was the presence
634 of corners and it is interesting to note that the limited phase trajectory convergence that
635 occurred in MIA animals may have been tied to the corners of the apparatus (see figure 5g).
636 Corners not only provide sensory information, but they require bidirectional modifications of
637 locomotor activity to navigate around them. Approximately one third of cells had significant
638 correlations of firing rate and speed, which is about half the figure reported by Wirtshafter
639 and Wilson (2019), but substantially more than that reported by Tingley and Buzsáki (2018).
640 The proportion of CTL group cells with firing rates that were negatively correlated with
641 speed was also just over half of all significantly correlated cells, in contrast to only around
642 one third in the Wirtshafter and Wilson (2019) study, suggesting that cells located in the
643 rostral LS may be particularly important for monitoring speed during tasks that involve
644 bidirectional speed fluctuations. Animals may have been able to move at a more constant
645 speed in the Tingley and Buzsáki (2018) due to the circular running apparatus.

646 A previous study from our lab showed that MIA disrupts theta sequences in the CA1
647 region of the hippocampus (Speers et al., 2021). According to predictions of the dynamic
648 weighting model proposed by Tingley and Buzsáki (2018), disrupted CA1 theta sequences
649 should prevent LS phase precession. However, in the current study, the proportion of cells
650 showing evidence of significant phase precession was not statistically different between
651 groups. Taken together, these data suggest that the MIA manipulation did not compromise
652 the ability of LS to precess relative to the CA1 theta oscillation, suggesting that upstream
653 disruptions of phase coding in the hippocampus do not abolish phase coding in the LS. They

654 may, however, interfere with how spatial information is discretized relative to reward
655 locations. Additional studies will be required, however, to test whether the MIA-induced
656 changes in LS phase precession are a direct result of disrupted theta sequences in the
657 hippocampus, or are reflective of some other change.

658 It is unclear what mechanism(s) might account for the steeper phase precession
659 observed in MIA animals. Our results showed that hippocampal theta frequency was
660 significantly slower in MIA animals, while at the same time the intrinsic burst frequency of
661 cells did not differ between groups, consistent with a 'detuned oscillator' (Drieu & Zugaro,
662 2019) explanation of the increase in phase precession slope. The magnitude of change
663 predicted by this model, did not, however, fully explain our observations. Alternatively,
664 according to somato-dendritic interference models (Drieu & Zugaro, 2019), an increase in the
665 rate of excitatory ramping onto LS neurons might produce the same effect, although this
666 ramping would have to be cyclic across the apparatus to produce the effect observed and
667 would fail to produce precession of greater than 180 degrees on a single pass.

668 These results provide further evidence that phase coding may be disturbed following
669 MIA (Speers et al., 2021), and suggest a biophysical mechanism for impaired integration of
670 contextual and reward information, which may explain why MIA animals display memory
671 impairments when multi-sensory integration is required (Ballentine et al., 2015; Howland,
672 Cazakoff, & Zhang, 2012). Impaired spatial-reward integration could also have profound
673 downstream effects on motivation and dopamine signalling, both of which are known to be
674 impaired in schizophrenia (Davis, Kahn, Ko, & Davidson, 1991; Strauss et al., 2013).
675 Consistent with this idea, a recent study has demonstrated that dysregulation of the CA1-LS
676 pathway induces both dopaminergic hyperactivity in the VTA and novelty-induced hyper-
677 locomotion that is schizophrenia-like, and that these could be attenuated via inhibition of the
678 LS (Zhang et al., 2022). The apparent smearing of reward representations across space, and

679 potentially time, by LS cells is also likely to compromise the development of conditioned
680 place preferences (Cazala et al., 1988; Jiang et al., 2018; Regier et al., 1990). It may also
681 underlie MIA-induced changes in reward and temporal processing (Deane, Millar, Bilkey, &
682 Ward, 2017; Millar, Bilkey, & Ward, 2017). The abnormal discretization of spatial
683 representations could also contribute to the impaired attentional filtering and aberrant
684 salience that have been described in schizophrenia (Kapur, 2003; Luck, Leonard, Hahn, &
685 Gold, 2019), and also in autism spectrum disorder (Bodner, Cowan, & Christ, 2019), another
686 MIA-associated neurodevelopmental disorder. (Haddad et al., 2020).

687

688

689

690

691

692

693

694

- 695 Adams, W., Kendell, R., Hare, E., & Munk-Jørgensen, P. (1993). Epidemiological evidence
696 that maternal influenza contributes to the aetiology of schizophrenia: An analysis of
697 Scottish, English, and Danish data. *The British Journal of Psychiatry*, 163(4), 522-
698 534.
- 699 Ballendine, S. A., Greba, Q., Dawicki, W., Zhang, X., Gordon, J. R., & Howland, J. G.
700 (2015). Behavioral alterations in rat offspring following maternal immune activation
701 and ELR-CXC chemokine receptor antagonism during pregnancy: implications for
702 neurodevelopmental psychiatric disorders. *Progress in Neuro-Psychopharmacology
703 and Biological Psychiatry*, 57, 155-165.
- 704 Bender, F., Gorbati, M., Cadavieco, M. C., Denisova, N., Gao, X., Holman, C., Korotkova,
705 T., & Ponomarenko, A. (2015). Theta oscillations regulate the speed of locomotion
706 via a hippocampus to lateral septum pathway. *Nature communications*, 6(1), 1-11.
- 707 Bitanhirwe, B. K., Peleg-Raibstein, D., Mouttet, F., Feldon, J., & Meyer, U. (2010). Late
708 prenatal immune activation in mice leads to behavioral and neurochemical
709 abnormalities relevant to the negative symptoms of schizophrenia.
710 *Neuropsychopharmacology*, 35(12), 2462.
- 711 Bodner, K. E., Cowan, N., & Christ, S. E. (2019). Contributions of filtering and attentional
712 allocation to working memory performance in individuals with autism spectrum
713 disorder. *Journal of abnormal psychology*, 128(8), 881.
- 714 Borhegyi, Z., Varga, V., Szilágyi, N., Fabo, D., & Freund, T. F. (2004). Phase segregation of
715 medial septal GABAergic neurons during hippocampal theta activity. *Journal of
716 Neuroscience*, 24(39), 8470-8479.
- 717 Brankač, J., Stewart, M., & Fox, S. E. (1993). Current source density analysis of the
718 hippocampal theta rhythm: associated sustained potentials and candidate synaptic
719 generators. *Brain research*, 615(2), 310-327.
- 720 Brébion, G., David, A. S., Pilowsky, L. S., & Jones, H. (2004). Recognition of visual stimuli
721 and memory for spatial context in schizophrenic patients and healthy volunteers.
722 *Journal of Clinical and Experimental Neuropsychology*, 26(8), 1093-1102.
- 723 Brown, A. S., & Meyer, U. (2018). Maternal immune activation and neuropsychiatric illness:
724 a translational research perspective. *American Journal of Psychiatry*, 175(11), 1073-
725 1083.
- 726 Buzsáki, G., Rappelsberger, P., & Kellényi, L. (1985). Depth profiles of hippocampal
727 rhythmic slow activity ('theta rhythm') depend on behaviour.
728 *Electroencephalography and clinical neurophysiology*, 61(1), 77-88.
- 729 Buzsáki, G., & Tingley, D. (2018). Space and time: The hippocampus as a sequence
730 generator. *Trends in cognitive sciences*, 22(10), 853-869.
- 731 Cazala, P., Galey, D., & Durkin, T. (1988). Electrical self-stimulation in the medial and
732 lateral septum as compared to the lateral hypothalamus: differential intervention of
733 reward and learning processes? *Physiology & behavior*, 44(1), 53-59.
- 734 Contreras, C. M., Dorantes, M. E., Mexicano, G., & Guzmán-Flores, C. (1986).
735 Lateralization of spike and wave complexes produced by hallucinogenic compounds
736 in the cat. *Experimental neurology*, 92(3), 467-478.
- 737 Dan, Y., & Poo, M.-m. (2004). Spike timing-dependent plasticity of neural circuits. *Neuron*,
738 44(1), 23-30.
- 739 Davis, K. L., Kahn, R. S., Ko, G., & Davidson, M. (1991). Dopamine in schizophrenia: a
740 review and reconceptualization. *The American journal of psychiatry*.
- 741 Deane, A. R., Millar, J., Bilkey, D. K., & Ward, R. D. (2017). Maternal immune activation in
742 rats produces temporal perception impairments in adult offspring analogous to those
743 observed in schizophrenia. *PloS one*, 12(11), e0187719.

- 744 Dickerson, D. D., Wolff, A. R., & Bilkey, D. K. (2010). Abnormal long-range neural
745 synchrony in a maternal immune activation animal model of schizophrenia. *Journal of*
746 *Neuroscience*, 30(37), 12424-12431.
- 747 Dragoi, G., & Buzsáki, G. (2006). Temporal encoding of place sequences by hippocampal
748 cell assemblies. *Neuron*, 50(1), 145-157.
- 749 Drieu, C., & Zugaro, M. (2019). Hippocampal Sequences During Exploration: Mechanisms
750 and Functions. *Frontiers in Cellular Neuroscience*, 13, 232.
- 751 Ekstrom, A., Meltzer, J., McNaughton, B., & Barnes, C. (2001). NMDA receptor antagonism
752 blocks experience-dependent expansion of hippocampal “place fields”. *Neuron*, 31(4),
753 631-638.
- 754 Fajnerová, I., Rodriguez, M., Levčík, D., Konrádová, L., Mikoláš, P., Brom, C., Stuchlík, A.,
755 Vlček, K., & Horáček, J. (2014). A virtual reality task based on animal research–
756 spatial learning and memory in patients after the first episode of schizophrenia.
757 *Frontiers in behavioral neuroscience*, 8, 157.
- 758 Feng, T., Silva, D., & Foster, D. J. (2015). Dissociation between the Experience-Dependent
759 Development of Hippocampal Theta Sequences and Single-Trial Phase Precession.
760 *Journal of Neuroscience*, 35(12), 4890-4902. doi:10.1523/Jneurosci.2614-14.2015
- 761 Foster, D. J., & Wilson, M. A. (2007). Hippocampal theta sequences. *Hippocampus*, 17(11),
762 1093-1099.
- 763 Geisler, C., Robbe, D., Zugaro, M., Sirota, A., & Buzsáki, G. (2007). Hippocampal place cell
764 assemblies are speed-controlled oscillators. *Proceedings of the National Academy of*
765 *Sciences*, 104(19), 8149-8154.
- 766 Glahn, D. C., Therman, S., Manninen, M., Huttunen, M., Kaprio, J., Lönnqvist, J., & Cannon,
767 T. D. (2003). Spatial working memory as an endophenotype for schizophrenia.
768 *Biological psychiatry*, 53(7), 624-626.
- 769 Groenewegen, H., Vermeulen-Van der Zee, E. t., Te Kortschot, A., & Witter, M. (1987).
770 Organization of the projections from the subiculum to the ventral striatum in the rat.
771 A study using anterograde transport of Phaseolus vulgaris leucoagglutinin.
772 *Neuroscience*, 23(1), 103-120.
- 773 Gupta, A. S., Van Der Meer, M. A., Touretzky, D. S., & Redish, A. D. (2012). Segmentation
774 of spatial experience by hippocampal theta sequences. *Nature neuroscience*, 15(7),
775 1032.
- 776 Haddad, F., Patel, S., & Schmid, S. (2020). Maternal immune activation by Poly I: C as a
777 preclinical model for neurodevelopmental disorders: a focus on autism and
778 schizophrenia. *Neuroscience & Biobehavioral Reviews*.
- 779 Hanlon, F. M., Weisend, M. P., Hamilton, D. A., Jones, A. P., Thoma, R. J., Huang, M.,
780 Martin, K., Yeo, R. A., Miller, G. A., & Cañive, J. M. (2006). Impairment on the
781 hippocampal-dependent virtual Morris water task in schizophrenia. *Schizophrenia*
782 *research*, 87(1-3), 67-80.
- 783 Heath, R. G., & Peacock, J. (2013). ADDENDUM E. ELECTROENCEPHALOGRAMS
784 AND SUBCORTICOGRAMS RECORDED SINCE THE JUNE 1952 MEETINGS.
785 In *Studies in Schizophrenia* (pp. 573-608): Harvard University Press.
- 786 Heath, R. G., & Walker, C. F. (1985). Correlation of deep and surface electroencephalograms
787 with psychosis and hallucinations in schizophrenics: a report of two cases. *Biological*
788 *psychiatry*.
- 789 Heusser, A. C., Poeppel, D., Ezzyat, Y., & Davachi, L. (2016). Episodic sequence memory is
790 supported by a theta–gamma phase code. *Nature neuroscience*, 19(10), 1374.
- 791 Howe, A. G., & Blair, H. T. (2020). Excitatory and inhibitory modulation of septal and
792 striatal neurons during hippocampal sharp-wave ripple events. *bioRxiv*.

- 793 Howland, J., Cazakoff, B., & Zhang, Y. (2012). Altered object-in-place recognition memory,
794 prepulse inhibition, and locomotor activity in the offspring of rats exposed to a viral
795 mimetic during pregnancy. *Neuroscience*, *201*, 184-198.
- 796 Huxter, J., Burgess, N., & O'Keefe, J. (2003). Independent rate and temporal coding in
797 hippocampal pyramidal cells. *Nature*, *425*(6960), 828-832.
- 798 Jaramillo, J., & Kempter, R. (2017). Phase precession: a neural code underlying episodic
799 memory? *Current opinion in neurobiology*, *43*, 130-138.
- 800 Jensen, J., Willeit, M., Zipursky, R. B., Savina, I., Smith, A. J., Menon, M., Crawley, A. P.,
801 & Kapur, S. (2008). The formation of abnormal associations in schizophrenia: neural
802 and behavioral evidence. *Neuropsychopharmacology*, *33*(3), 473.
- 803 Jiang, J. X., Liu, H., Huang, Z. Z., Cui, Y., Zhang, X. Q., Zhang, X. L., Cui, Y., & Xin, W. J.
804 (2018). The role of CA3-LS-VTA loop in the formation of conditioned place
805 preference induced by context-associated reward memory for morphine. *Addiction*
806 *biology*, *23*(1), 41-54.
- 807 Kamondi, A., Acsády, L., Wang, X. J., & Buzsáki, G. (1998). Theta oscillations in somata
808 and dendrites of hippocampal pyramidal cells in vivo: Activity-dependent phase-
809 precession of action potentials. *Hippocampus*, *8*(3), 244-261.
- 810 Kapur, S. (2003). Psychosis as a state of aberrant salience: a framework linking biology,
811 phenomenology, and pharmacology in schizophrenia. *American Journal of*
812 *Psychiatry*, *160*(1), 13-23.
- 813 Kempter, R., Leibold, C., Buzsáki, G., Diba, K., & Schmidt, R. (2012). Quantifying circular-
814 linear associations: Hippocampal phase precession. *Journal of neuroscience methods*,
815 *207*(1), 113-124.
- 816 Kjelstrup, K. B., Solstad, T., Brun, V. H., Hafting, T., Leutgeb, S., Witter, M. P., Moser, E. I.,
817 & Moser, M.-B. (2008). Finite scale of spatial representation in the hippocampus.
818 *Science*, *321*(5885), 140-143.
- 819 Lubenov, E. V., & Siapas, A. G. (2009). Hippocampal theta oscillations are travelling waves.
820 *Nature*, *459*(7246), 534.
- 821 Luck, S. J., Leonard, C. J., Hahn, B., & Gold, J. M. (2019). Is Attentional Filtering Impaired
822 in Schizophrenia? *Schizophrenia bulletin*, *45*(5), 1001-1011.
- 823 Luo, A. H., Tahsili-Fahadan, P., Wise, R. A., Lupica, C. R., & Aston-Jones, G. (2011).
824 Linking context with reward: a functional circuit from hippocampal CA3 to ventral
825 tegmental area. *Science*, *333*(6040), 353-357.
- 826 Magee, J. C. (2001). Dendritic mechanisms of phase precession in hippocampal CA1
827 pyramidal neurons. *Journal of neurophysiology*, *86*(1), 528-532.
- 828 Maurer, A. P., Cowen, S. L., Burke, S. N., Barnes, C. A., & McNaughton, B. L. (2006).
829 Organization of hippocampal cell assemblies based on theta phase precession.
830 *Hippocampus*, *16*(9), 785-794.
- 831 Mehta, M., Lee, A., & Wilson, M. (2002). Role of experience and oscillations in
832 transforming a rate code into a temporal code. *Nature*, *417*(6890), 741.
- 833 Millar, J., Bilkey, D. K., & Ward, R. D. (2017). Maternal immune activation alters sensitivity
834 to action-outcome contingency in adult rat offspring. *Brain, behavior, and immunity*,
835 *63*, 81-87.
- 836 O'keefe, J., & Nadel, L. (1978). *The hippocampus as a cognitive map*: Oxford: Clarendon
837 Press.
- 838 O'Keefe, J., & Recce, M. L. (1993). Phase relationship between hippocampal place units and
839 the EEG theta rhythm. *Hippocampus*, *3*(3), 317-330.
- 840 Park, S., & Holzman, P. S. (1992). Schizophrenics show spatial working memory deficits.
841 *Archives of general psychiatry*, *49*(12), 975-982.

- 842 Paxinos, G., & Watson, C. (2006). *The rat brain in stereotaxic coordinates: hard cover*
843 *edition*: Elsevier.
- 844 Qasim, S. E., Fried, I., & Jacobs, J. (2020). Phase precession in the human hippocampus and
845 entorhinal cortex. *bioRxiv*.
- 846 Regier, D. A., Farmer, M. E., Rae, D. S., Locke, B. Z., Keith, S. J., Judd, L. L., & Goodwin,
847 F. K. (1990). Comorbidity of mental disorders with alcohol and other drug abuse:
848 results from the Epidemiologic Catchment Area (ECA) study. *Jama*, *264*(19), 2511-
849 2518.
- 850 Risold, P., & Swanson, L. (1997). Connections of the rat lateral septal complex. *Brain*
851 *Research Reviews*, *24*(2-3), 115-195.
- 852 Rizzo, L., Danion, J.-M., Van Der Linden, M., Grangé, D., & Rohmer, J.-G. (1996).
853 Impairment of memory for spatial context in schizophrenia. *Neuropsychology*, *10*(3),
854 376.
- 855 Royer, S., Sirota, A., Patel, J., & Buzsáki, G. (2010). Distinct representations and theta
856 dynamics in dorsal and ventral hippocampus. *Journal of Neuroscience*, *30*(5), 1777-
857 1787.
- 858 Salgado-Pineda, P., Landin-Romero, R., Portillo, F., Bosque, C., Pomes, A., Spanlang, B.,
859 Franquelo, J. C., Teixido, C., Sarró, S., & Salvador, R. (2016). Examining
860 hippocampal function in schizophrenia using a virtual reality spatial navigation task.
861 *Schizophrenia research*, *172*(1-3), 86-93.
- 862 Savanthrapadian, S., Wolff, A. R., Logan, B. J., Eckert, M. J., Bilkey, D. K., & Abraham, W.
863 C. (2013). Enhanced hippocampal neuronal excitability and LTP persistence
864 associated with reduced behavioral flexibility in the maternal immune activation
865 model of schizophrenia. *Hippocampus*, *23*(12), 1395-1409.
- 866 Schmidt, R., Diba, K., Leibold, C., Schmitz, D., Buzsáki, G., & Kempter, R. (2009). Single-
867 trial phase precession in the hippocampus. *Journal of Neuroscience*, *29*(42), 13232-
868 13241.
- 869 Sheehan, T. P., Chambers, R. A., & Russell, D. S. (2004). Regulation of affect by the lateral
870 septum: implications for neuropsychiatry. *Brain Research Reviews*, *46*(1), 71-117.
- 871 Skaggs, W. E., McNaughton, B. L., & Gothard, K. M. (1993). *An information-theoretic*
872 *approach to deciphering the hippocampal code*. Paper presented at the Advances in
873 neural information processing systems.
- 874 Skaggs, W. E., McNaughton, B. L., Wilson, M. A., & Barnes, C. A. (1996). Theta phase
875 precession in hippocampal neuronal populations and the compression of temporal
876 sequences. *Hippocampus*, *6*(2), 149-172.
- 877 Speers, L. J., Cheyne, K. R., Cavani, E., Hayward, T., Schmidt, R., & Bilkey, D. K. (2021).
878 Hippocampal sequencing mechanisms are disrupted in a maternal immune activation
879 model of schizophrenia risk. *The Journal of Neuroscience*, JN-RM-0730-0721.
880 doi:10.1523/jneurosci.0730-21.2021
- 881 Strauss, G. P., Waltz, J. A., & Gold, J. M. (2013). A review of reward processing and
882 motivational impairment in schizophrenia. *Schizophrenia bulletin*, *40*(Suppl_2),
883 S107-S116.
- 884 Swanson, L., & Cowan, W. (1977). An autoradiographic study of the organization of the
885 efferent connections of the hippocampal formation in the rat. *Journal of Comparative*
886 *Neurology*, *172*(1), 49-84.
- 887 Takamura, Y., Tamura, R., Zhou, T. L., Kobayashi, T., Tran, A. H., Eifuku, S., & Ono, T.
888 (2006). Spatial firing properties of lateral septal neurons. *Hippocampus*, *16*(8), 635-
889 644.
- 890 Terada, S., Sakurai, Y., Nakahara, H., & Fujisawa, S. (2017). Temporal and rate coding for
891 discrete event sequences in the hippocampus. *Neuron*, *94*(6), 1248-1262. e1244.

892 Terrazas, A., Krause, M., Lipa, P., Gothard, K. M., Barnes, C. A., & McNaughton, B. L.
893 (2005). Self-motion and the hippocampal spatial metric. *Journal of Neuroscience*,
894 25(35), 8085-8096.

895 Tingley, D., & Buzsáki, G. (2018). Transformation of a Spatial Map across the Hippocampal-
896 Lateral Septal Circuit. *Neuron*.

897 van der Meer, M. A., & Redish, A. D. (2011). Theta phase precession in rat ventral striatum
898 links place and reward information. *Journal of Neuroscience*, 31(8), 2843-2854.

899 Wang, Y., Romani, S., Lustig, B., Leonardo, A., & Pastalkova, E. (2015). Theta sequences
900 are essential for internally generated hippocampal firing fields. *Nature neuroscience*,
901 18(2), 282.

902 Waters, F. A., Maybery, M. T., Badcock, J. C., & Michie, P. T. (2004). Context memory and
903 binding in schizophrenia. *Schizophrenia research*, 68(2-3), 119-125.

904 Weniger, G., & Irle, E. (2008). Allocentric memory impaired and egocentric memory intact
905 as assessed by virtual reality in recent-onset schizophrenia. *Schizophrenia research*,
906 101(1-3), 201-209.

907 Whitton, A. E., Treadway, M. T., & Pizzagalli, D. A. (2015). Reward processing dysfunction
908 in major depression, bipolar disorder and schizophrenia. *Current opinion in*
909 *psychiatry*, 28(1), 7.

910 Wikenheiser, A. M., & Redish, A. D. (2015). Hippocampal theta sequences reflect current
911 goals. *Nature neuroscience*, 18(2), 289.

912 Wirtshafter, H. S., & Wilson, M. A. (2019). Locomotor and hippocampal processing
913 converge in the lateral septum. *Current Biology*, 29(19), 3177-3192. e3173.

914 Wirtshafter, H. S., & Wilson, M. A. (2020). Differences in reward biased spatial
915 representations in the lateral septum and hippocampus. *Elife*, 9, e55252.

916 Wirtshafter, H. S., & Wilson, M. A. (2021). Lateral Septum as a Nexus for Mood,
917 Motivation, and Movement. *Neuroscience & Biobehavioral Reviews*.

918 Wolff, A. R., & Bilkey, D. K. (2015). Prenatal immune activation alters hippocampal place
919 cell firing characteristics in adult animals. *Brain, behavior, and immunity*, 48, 232-
920 243.

921 Wolff, A. R., Cheyne, K. R., & Bilkey, D. K. (2011). Behavioural deficits associated with
922 maternal immune activation in the rat model of schizophrenia. *Behavioural brain*
923 *research*, 225(1), 382-387.

924 Yu, B., Wang, C., Liu, J., Johnson, K., & Gallagher, J. (2002). Adaptation to chronic PCP
925 results in hyperfunctional NMDA and hypofunctional GABAA synaptic receptors.
926 *Neuroscience*, 113(1), 1-10.

927 Zhang, J., Navarrete, M., Wu, Y., & Zhou, Y. (2022). 14-3-3 Dysfunction in Dorsal
928 Hippocampus CA1 (dCA1) Induces Psychomotor Behavior via a dCA1-Lateral
929 Septum-Ventral Tegmental Area Pathway. *Frontiers in Molecular Neuroscience*, 15.

930 Zhou, T. L., Tamura, R., Kuriwaki, J., & Ono, T. (1999). Comparison of medial and lateral
931 septal neuron activity during performance of spatial tasks in rats. *Hippocampus*, 9(3),
932 220-234.

933

934

935

936 **Figure 1.** Methodological details and verification of electrode placement. (a) Diagram of the
937 rectangular track. Rats were pre-trained to run in a clockwise direction for a food reward delivered at
938 the centre of the bottom arm (marked with the red X). (b) Tetrode placement in the LS (highlighted in
939 yellow). The tetrodes bundles are depicted by the thick black line. Dashed purple lines indicate the
940 initial depth of electrode placement during surgery, while red lines show the range of target location
941 through the rostral LS over the course of the experiment. (c) Diagram of the hippocampus showing
942 the target area for LFP surgical implantation, and an example photograph of histology demonstrating
943 electrode placement in the pyramidal cell layer of CA1. (d) Cluster cutting examples for CTL cells
944 (shown in blue) and MIA (yellow). These examples show some of the different spike widths and
945 inter-spike interval histogram profiles observed in the LS. The top CTL example is similar to a
946 canonical place field, while the second CTL cell has a similar waveform, but the histogram profile
947 shows a more continuous spiking pattern across time. The first MIA example shows a cell with a
948 narrower waveform and a delayed spiking profile, whereas the final example shows a broader
949 waveform, similar to a hippocampal place cell, but the spiking profile is more reminiscent of an
950 interneuron. These spiking profiles were common across both groups, and were chosen to demonstrate
951 the range of different spiking profiles observed rather than systematic group differences. (e)
952 Schematic of final tetrode location in the LS for CTL animals at the termination of the experiment.
953 Modified stereotaxic image taken from Paxinos and Watson (2006). Percentages refer to the
954 proportion of phase coding cells calculated individually for each animal, with phase coding cells
955 defined as cells with a significant ($<.05$) circular-linear correlation of phase and position. Faded red
956 areas delineate regions where less than 20% of all recorded cells demonstrated evidence of significant
957 phase precession, and faded yellow delineates regions where proportions fell between 21 and 40%.
958 Example images of tetrode placement in the rostral LS is shown below. The second example shows
959 the final electrode placement of the excluded cell in the MS (marked with a cross). Additional
960 inspection of firing rates of the excluded cell compared to all other cells demonstrated that they were
961 atypical (below right). (f) As for e, but for MIA cells.

962

963 **Figure 2.** Basic firing properties of LS cells, mean locomotor speed, and comparison of
964 hippocampal theta properties. (a) Median firing rate of LS cells across the entire track. (b) Information
965 content of LS cells, measured in bits/spike. Bar denotes median values. (c) Mean locomotor speed as
966 animals traversed the rectangular track. Bars denote mean and SEM. (d) EEG amplitude of CA1 LFP
967 recordings. Error bars denote mean and SEM. (e) Examples of filtered and raw EEG recordings for
968 both groups. (f) Violin plots of theta frequency in Hz. (g) Average wave form shape of CA1 LFP
969 oscillations in the theta band. Lighter colour denotes standard error. (h) Average phase profile of the
970 theta waveform, from the Hilbert transform. (i) Comparison of median r values for the theta
971 frequency/ speed correlations generated for each individual recording.
972
973
974

975 **Figure 3.** Comparison of LS phase precession between CTL and MIA animals. (a) Example
976 plots of phase precession in CTL cells. These examples were chosen to demonstrate a range of phase
977 precession (PP) variability, and each example cell is taken from a different animal. For each example
978 cell, the figure on the left displays PP as a function of colour around the track, with dark blue
979 representative of 0° and red representative of 360° . On the right are the corresponding PP plots after
980 linearization of the track for selected segments. Red lines denote the regression slope. In all plots,
981 phase is repeated across 2 cycles for clarity. In the CTL group, example cell 1 demonstrates both
982 spatially selective firing around half of the track in addition to robust PP. Example cell 2 demonstrates
983 robust phase precession across the majority of the track, with PP around 1 full cycle. Example cell 3
984 demonstrates robust PP through the reward area. Example cell 4 demonstrates a shallow PP slope and
985 sparse firing outside the reward area. (b) As for (a), but for example MIA cells. Example cell 1
986 demonstrates robust PP that approaches a full cycle. Example cell 2 demonstrates robust PP across the
987 entire track, in which PP appears to reset at the top left-hand corner. Example cell 3 demonstrates
988 robust PP through multiple cycles across the track. Example cell 4 demonstrates robust PP that
989 precesses through 2 distinct cycles.

990

991 **Figure 4.** LS cells in the MIA group are more likely to precess across multiple theta cycles.
992 (a) Proportion of LS cells with statistically significant ($p < .05$) phase precession for each group. (b)
993 Mean r values of the circular correlation of phase and position for both groups. Error bars denote
994 SEM. (c) p values of the circular linear correlation shown in (b). (d) Slope values (deg/mm) for all
995 cells (on right), and for a subset of cells demonstrating significant phase precession (on left). Black
996 lines denote median values. (e) Phase cycles across the full track. Error bars denote median with 95%
997 confidence intervals. (f) Mean slope values of the circular-linear correlation on an animal by animal
998 basis. Error bars denote SEM. (g) Log transformed firing rates of the subset of cells demonstrating
999 significant phase precession. Error bars denote mean and SEM. (h) Theta burst frequency of single
1000 units. (i) Circular histograms of intercept values for both groups, demonstrating greater variability of
1001 phase precession starting phase in the MIA group. Between group differences are based on the
1002 variance ratio F test. Red bars denote the mean angle with 95% confidence intervals.

1003

1004

1005 **Figure 5.** Relationship between firing phase and reward. (a) Correlations of LS electrode
1006 depth and lead/lag of LFPs recorded simultaneously from CA1 and the LS. Each animal is shown in a
1007 different color. Negative values indicate that the LS is leading CA1, and positive values indicate that
1008 CA1 is leading the LS. (b) Example of phase correction shift. (c) Phase trajectories of each precessing
1009 LS CTL group cell (as in figure 3a). Each trajectory is plotted onto one diagram where x-axis is
1010 linearized track. Vertical lines indicate corners and triangle marks reward location. Note how many
1011 tracks seem to pass through phase/location point at around 180° phase at the reward location. (d)
1012 Clustering of phase trajectories in the CTL group (from data in c), measured as mean vector length
1013 (MVL; y-axis), across the track (x-axis). Mean vector length can vary from 0 – no clustering to 1 -
1014 tight clustering or focus. Note that control trajectories show greatest clustering (phase focus) at the
1015 reward location (triangle). (e) Circular histogram of corrected phase angle (as shown in shown in c)
1016 when measured at the reward location. (f) Phase trajectory of each MIA group cell (as in figure 3b).
1017 Note that there is no clear clustering of phase trajectories around the reward location. (g) As in d, but
1018 for the MIA group. In contrast to the CTL group, MIA trajectories show much less clustering, with
1019 very little clustering at the reward location and less differentiation across the track. (h) As for e, but
1020 for MIA phase angles.
1021
1022

1023 **Figure 6.** Evidence of speed modulated cells in the rostral LS. (a) Example plots
1024 demonstrating robust correlations of firing rate and speed for both groups (first 3 examples in each
1025 row). The final example in each row shows firing rates that were correlated with acceleration rather
1026 than speed. These examples were chosen to demonstrate both positive and negative correlations that
1027 were typically observed across both groups. (b) Proportion of cells with significant correlations of
1028 firing rate and speed. Significance level for the linear correlation was set at 0.05. Sig. + refers to
1029 significant positive correlations and sig. - refers to negative correlations. (c) Violin plots of the
1030 absolute r value of the firing rate/speed correlation for the entire dataset (left column). Median r
1031 values for the linear correlation of firing rate and speed when only those cells with a significant firing
1032 rate/speed correlation were included are shown on the right. Error bars include 95% confidence
1033 intervals (d) As for (b), but including cells with significant phase precession to demonstrate
1034 overlapping cell properties. (e) As for c, but for acceleration (+) and deceleration (-). Error bars
1035 denote mean and SEM.

1036

1037

1038

1039 **Figure 7.** Schematic of LS phase precession in CTL and MIA animals. In the CTL diagram,
1040 phase of LS cell firing (PP; coded by colour) occurs across a single cycle as the animal traverses a
1041 familiar route to a reward. In the upper rectangle, the range of PP from the starting location (S) is
1042 determined by a salient external cue marking the end of the route (white square) while other external
1043 cues (grey squares) and the reward itself (grey star) do not affect PP range. Alternatively in the lower
1044 example, PP range is anchored to the reward (white R) itself, while external cues are irrelevant. In
1045 both cases, intact theta sequences(A-D) arriving from CA1 (and potentially CA3) are likely to
1046 contribute to the emergence of single cycle PP in the LS and phase-coded information about the
1047 likelihood of rewards across the trajectory could be transmitted to subcortical regions such as the
1048 VTA. In the MIA example, disordered theta sequences from CA1 (and potentially CA3) may
1049 contribute to PP in the LS that exceeds a single theta cycle as the animal traverses a familiar route.
1050 The range of PP may be anchored to several salient cues across the trajectory (white squares),
1051 providing a more discretized representation of a navigational route in comparison to CTL animals.
1052 Alternatively, multiple cycle PP in MIA animals may reflect erroneous reward expectancies as the
1053 animal traverses the route. As a result, information about incorrect reward expectancies (red arrows)
1054 may be transmitted to the VTA, which could contribute to abnormal dopamine signalling in
1055 subcortical regions.

1056

1057

1058

1059

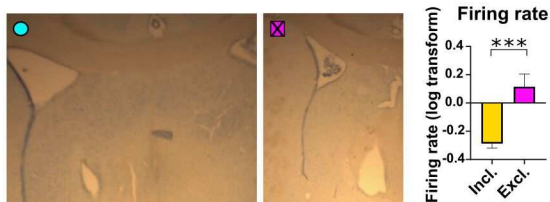
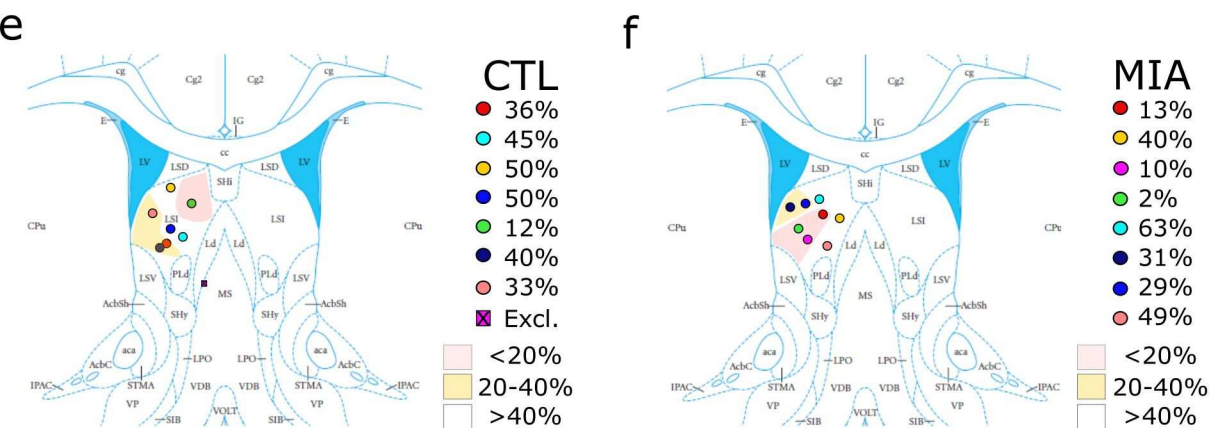
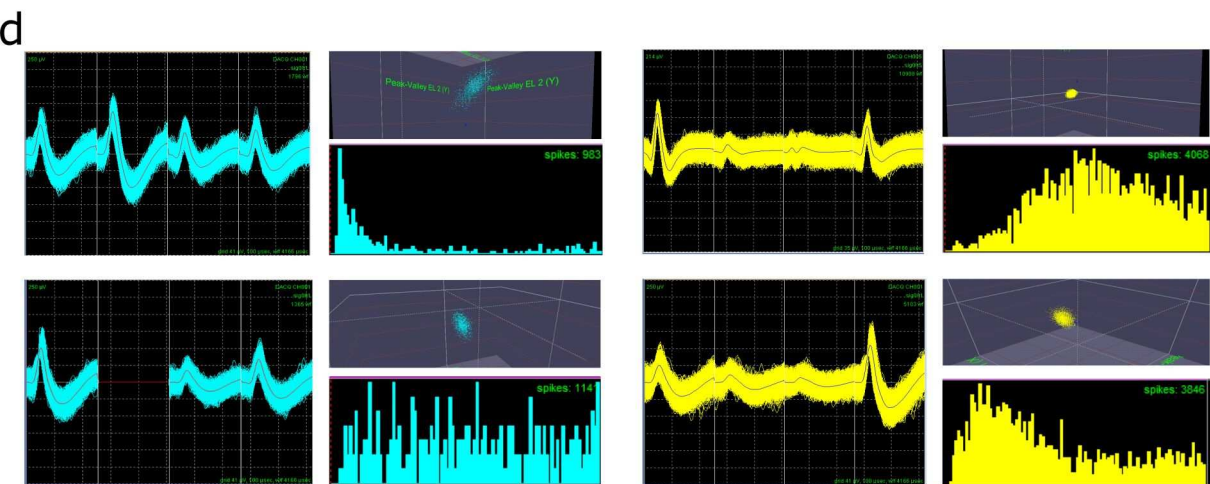
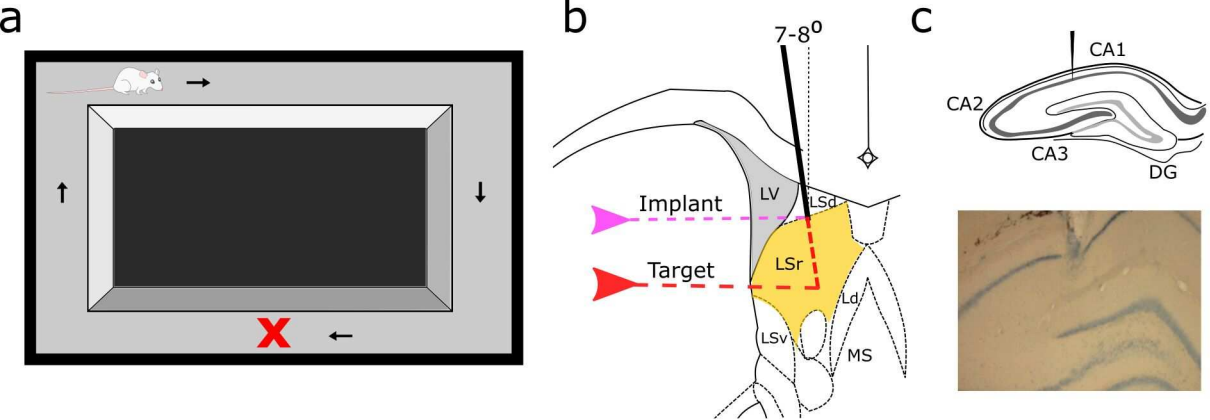
1060

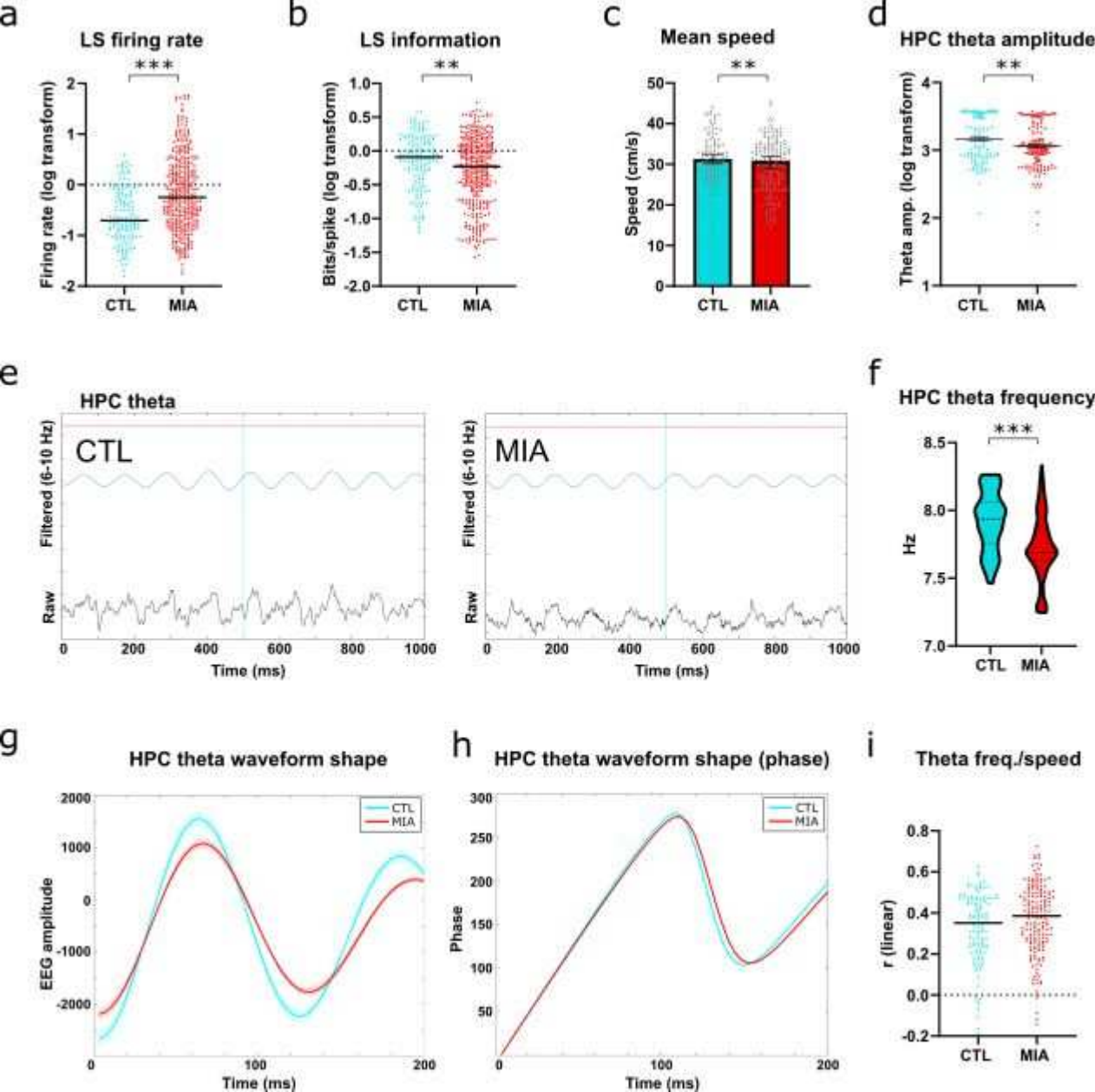
1061

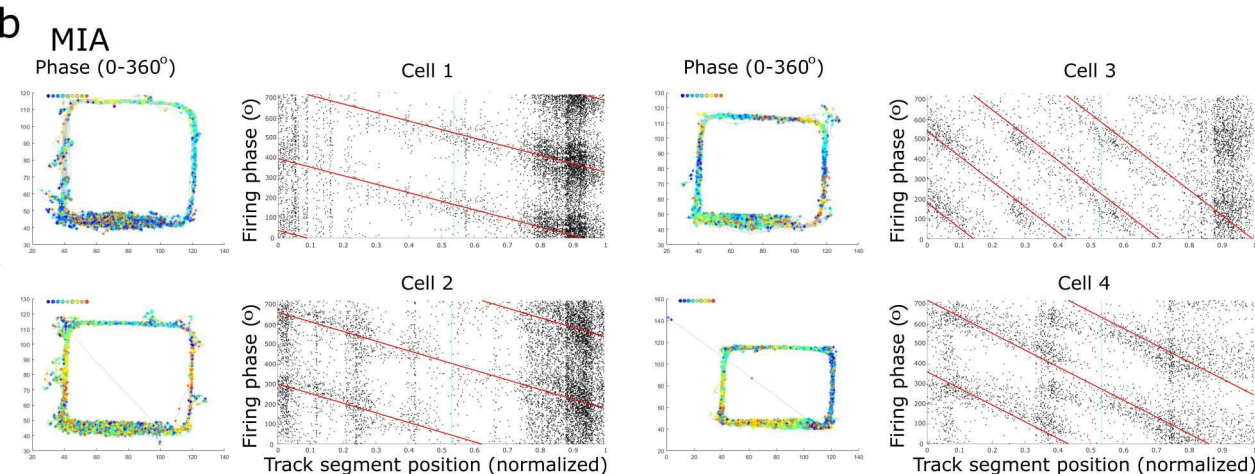
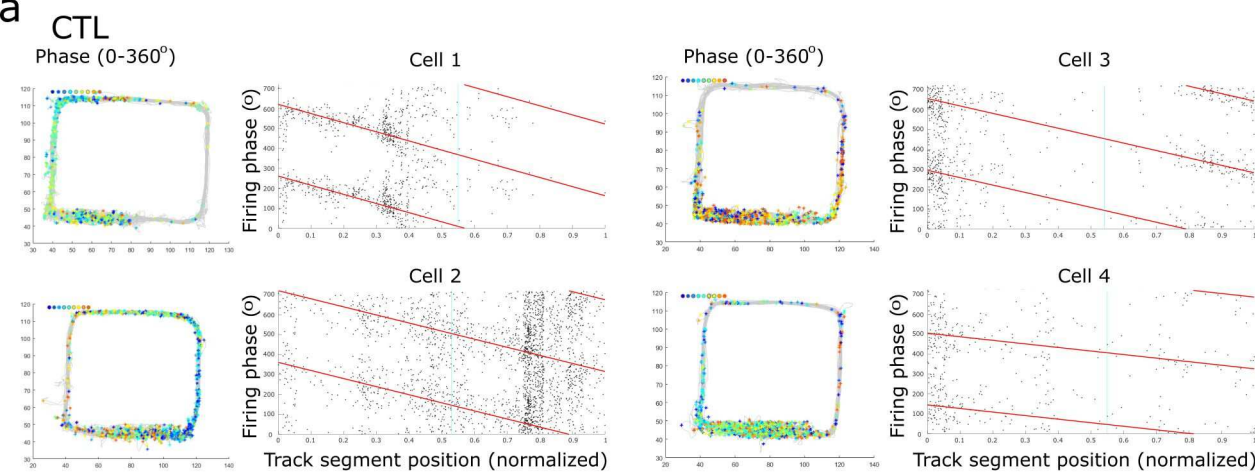
1062

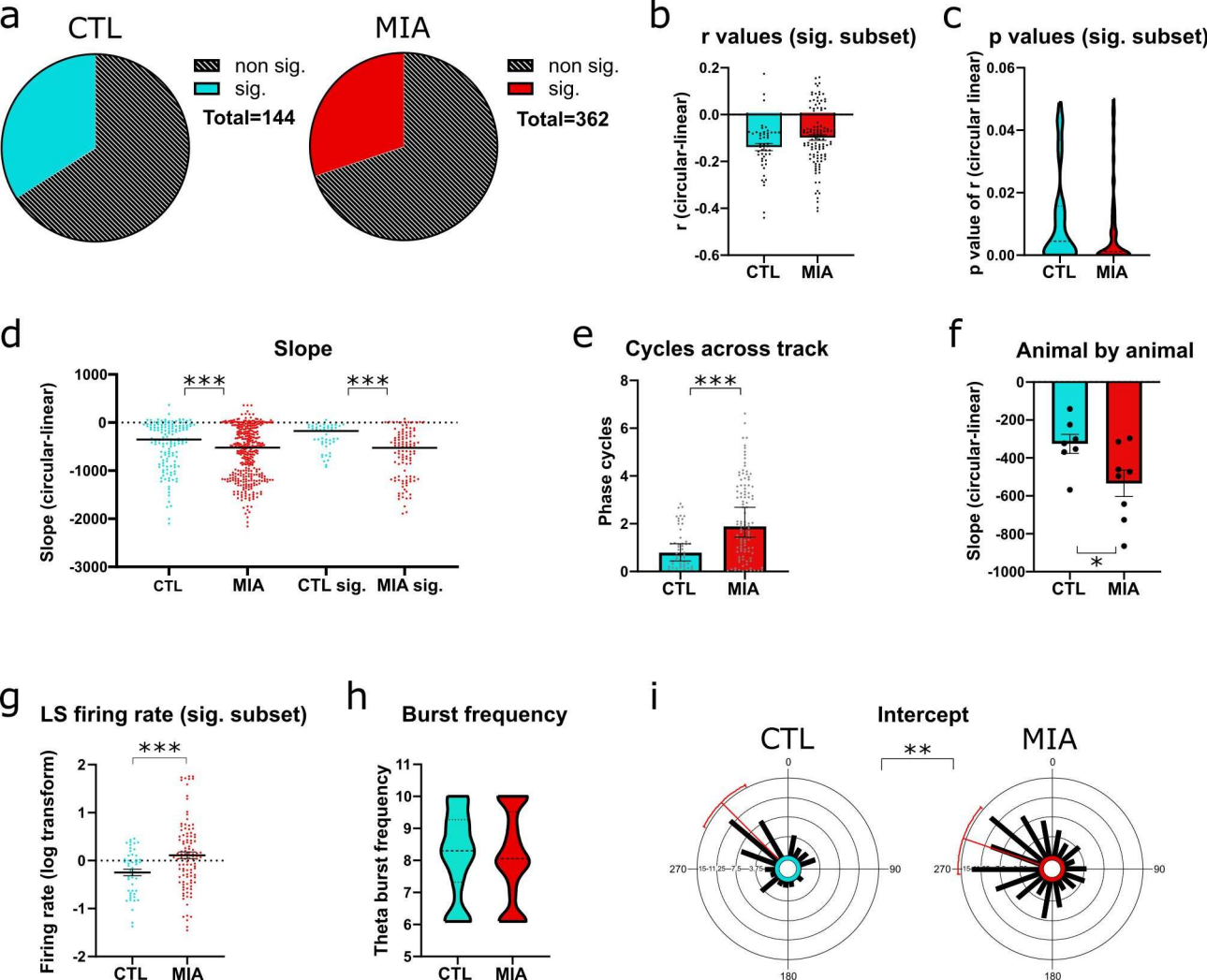
1063

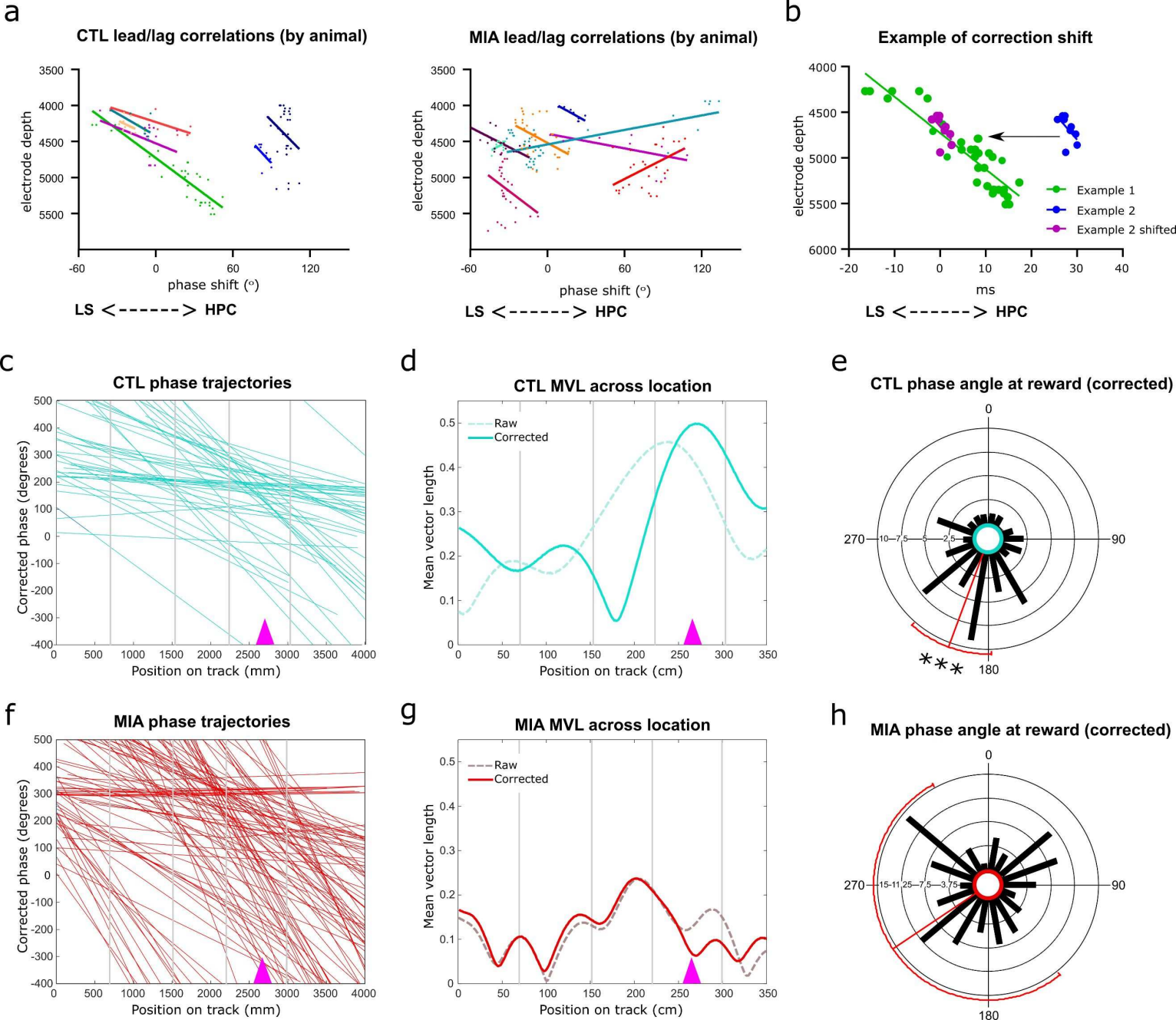
1064

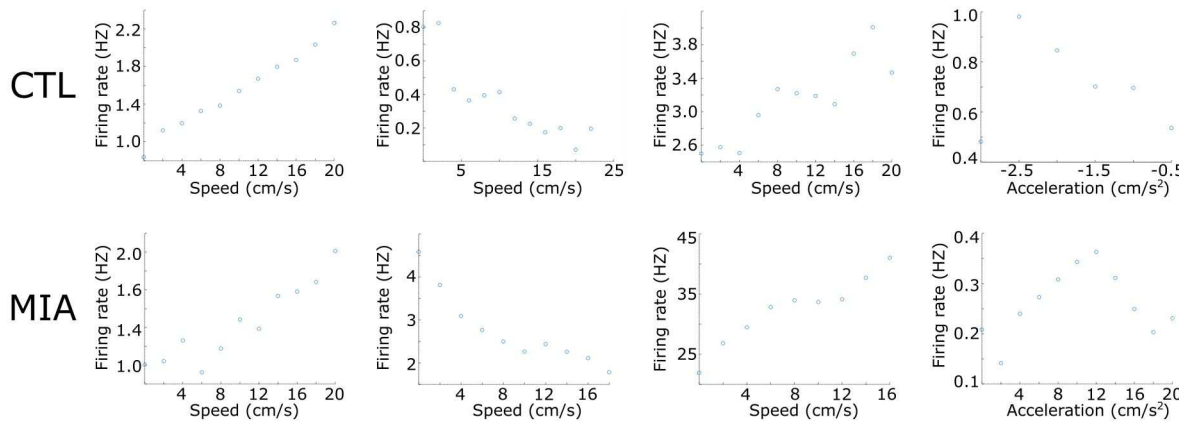
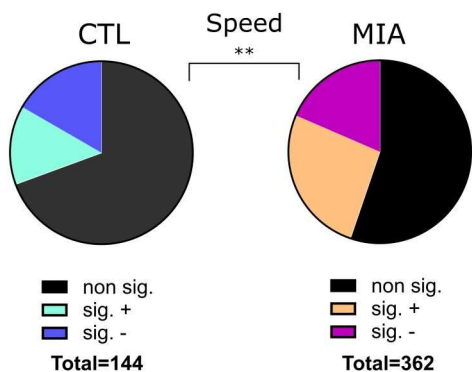
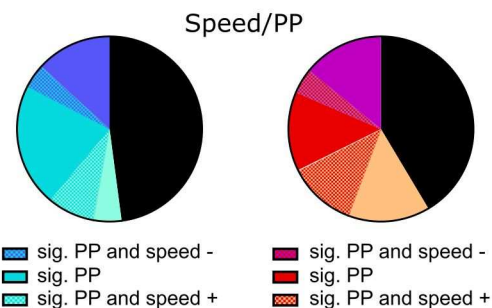
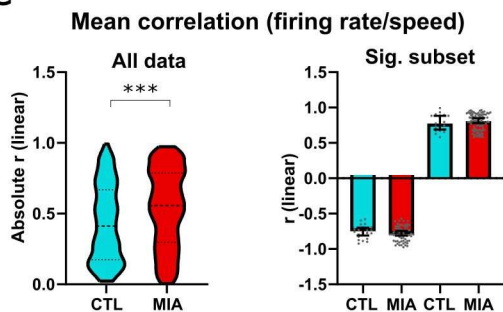










a**b****d****c****e**